

Generalised route to effective field theories for quantum systems with local constraints

Attila Szabó,¹ Garry Goldstein,² Claudio Castelnovo,¹ and Alexei M. Tsvelik³

¹*TCM Group, Cavendish Laboratory, University of Cambridge,
J. J. Thomson Avenue, Cambridge CB3 0HE, United Kingdom*

²*Physics and Astronomy Department, Rutgers University, Piscataway, NJ 08854, USA*

³*Condensed Matter Physics and Materials Science Division,
Brookhaven National Laboratory, Upton, NY 11973-5000, USA*

Some of the exciting phenomena uncovered in strongly correlated systems in recent years – for instance quantum topological order, deconfined quantum criticality, and emergent gauge symmetries – appear in systems in which the Hilbert space is effectively projected at low energies in a way that imposes local constraints on the original degrees of freedom. Cases in point include spin liquids, valence bond systems, dimer models, and vertex models. In this work, we use a slave boson description coupled to a large- S path integral formulation to devise a generalised route to obtain effective field theories for such systems. We demonstrate the validity and capability of our approach by studying quantum dimer models and by comparing our results with the existing literature. Field-theoretic approaches to date are limited to bipartite lattices, they depend on a gauge-symmetric understanding of the constraint, and they lack generic quantitative predictive power for the coefficients of the terms that appear in the Lagrangians of these systems. Our method overcomes all these shortcomings and we show how the results up to quadratic order compare with the known height description of the square lattice quantum dimer model, as well as with the numerical estimate of the speed of light of the photon excitations on the diamond lattice. Finally, instanton considerations allow us to infer properties of the finite-temperature behaviour in two dimensions.

I. INTRODUCTION

Low-energy descriptions of strongly correlated many-body systems sometimes require the introduction of projected Hilbert spaces where the degrees of freedom are subject to local constraints. Notable examples include valence bond systems, quantum dimer models, and vertex models. The action of the system Hamiltonian within the restricted Hilbert space often gives rise to exotic and unexpected behaviour, from emergent gauge symmetries and deconfined quantum criticality to quantum topological order, which have been the subject of much attention in recent years.

Field-theoretic descriptions of these systems have proven to be a powerful tool to study their properties, in particular to understand the nature of their correlations and critical points. However, conventional routes to construct such field theories often do not apply, and instead ad hoc methods have been devised throughout the years. Such methods largely hinge on a physical understanding of the constraint and how to best represent it in a (free) field theory language. While on the one hand such approaches have provided great insight into the relevant systems, they cannot easily be generalised. A systematic way to arrive at a field-theoretic description of quantum systems with local constraints is currently lacking.

In this paper, we propose a generalised route to obtain field-theoretic actions from microscopic Hamiltonians based on a slave boson representation of the relevant degrees of freedom and their constraints, combined with a large- S path integral formulation. We demonstrate the validity and capability of our approach by deploying it to study quantum dimer models (QDMs), recovering known and obtaining new results on bipartite lattices, and showing that it can be used straightforwardly on hitherto inaccessible non-bipartite lattices. Our approach also paves the way to semiclassical simulations of these systems, as discussed in Ref. 1 by some of the authors.

QDMs were introduced to describe a magnetically disordered (resonating valence bond) phase in high-temperature superconducting materials [2]. They can also arise in Bose–Mott insulators, electronic Mott insulators at fractional fillings [3], and in mixed valence systems on frustrated lattices [4]. For a review of these models, we refer the reader to Ref. 5.

When QDMs are defined on bipartite lattices, they are amenable to a height mapping description in two dimensions (2D), which generalises to quantum electrodynamics (QED) in 3D [5–8]. The height mapping is built upon a gauge-symmetric understanding of the constraint [9] and has great predictive power for bipartite quantum dimer models, enabling one to answer detailed questions pertaining to their long-wavelength properties. All its good features notwithstanding, the height mapping has one essential drawback: a quantitative derivation of its action from the microscopic lattice Hamiltonian is currently not available. The state-of-the-art derivation of the height mapping has been so far phenomenological [5, 10], and the coefficients (including their signs) are *a posteriori* determined by theoretical considerations (e.g., using the knowledge of the exact ground state at fine-tuned critical points) combined with comparisons to numerical results [5–8, 10, 11]. Furthermore, the approach cannot be applied to nonbipartite lattices, which remain comparatively unexplored from a field-theoretic perspective.

Using our generalised route, we show that one can systematically derive the height Lagrangian for bipartite QDMs in 2D and 3D, from the corresponding microscopic Hamiltonians. We compare our results against the existing literature, where we find good agreement considering the large- S and quadratic approximations that we employ. For example, we derive the stiffness of the 2D square lattice QDM at a well-known critical point called the Rokhsar–Kivelson (RK) point [2], where the ground-state wave function of the system is known exactly: Our result, $1/4$, is comparable to

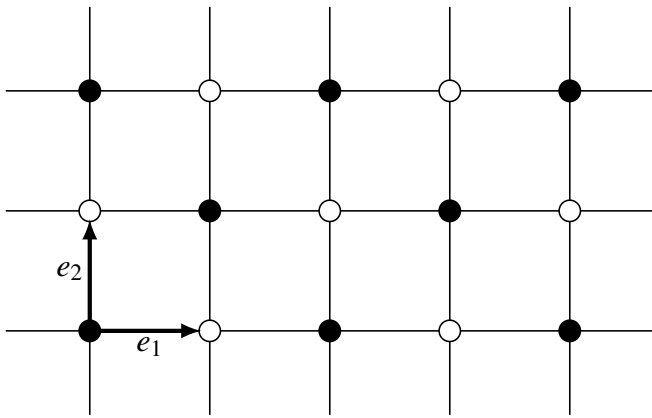


FIG. 1. Square lattice showing the choice of basis vectors $e_{1,2}$.

the exact value, $\pi/18$ [5, 12]. We use instanton considerations to discuss the fate of 2D phases at finite temperature. We also obtain the speed of light to quadratic order in the 3D QED long-wavelength theory of dimers on the cubic lattice, $c = \sqrt{2J(J-V)}S/3$, and on the diamond lattice, $c = \sqrt{J(J-V)/6}S^2$. The latter is known numerically from quantum Monte Carlo simulations to be $c(S=1) \simeq \sqrt{0.8J(J-V)}$ [13, 14]. We further show that our approach applies straightforwardly to the non-bipartite case of the QDM on the triangular lattice, where we observe a curious analytical similarity with the formalism for the QDM on the 3D cubic lattice – a similarity that we plan to explore further in future work.

The paper is organised as follows. In Sec. II, we introduce our approach by studying in detail the introductory and well-known case of the QDM on the square lattice. In Sec. III, we study the cubic lattice and obtain the dispersion of its photon excitations in the gapless phase. We then briefly consider the case of the nonbipartite triangular lattice in Sec. IV, which is shown to be curiously similar in its analytical form to the cubic lattice. Finally, in Secs. V and VI, we consider for completeness the QDMs on the honeycomb and diamond lattices, respectively. A comparison with the conventional height mapping and gauge theoretic formulations is presented in Sec. VII, and we conclude in Sec. VIII.

II. SQUARE LATTICE

A. Bosonic representation and large S

We consider in the first instance the well-known case of the RK Hamiltonian for the square lattice QDM, which allows us to introduce our approach in the simplest setting. Generalisa-

tions to the honeycomb, triangular, cubic and diamond lattices will be discussed in later sections.

The quantum dimer model can be mapped exactly onto a slave boson model by considering a secondary Hilbert space where we assign a bosonic mode $b_{r,\eta}$ to each link $(r, r + e_\eta)$ of the square lattice ($e_\eta = \hat{x}, \hat{y}$) [15] (see Fig. 1). We associate the number of dimers on a link with the occupation number of the bosons on that link, thus embedding the dimer Hilbert space in the larger Hilbert space of the bosons.

The constraint that each site of the lattice has one and exactly one dimer attached to it can be expressed in the boson language as

$$\Pi_r \equiv \sum_{\ell \in \nu_r} b_\ell^\dagger b_\ell - 1 = 0. \quad (2.1)$$

Here, for convenience of notation, $\ell \in \nu_r$ labels the four links r', η that are attached to the vertex r . We note that the constraint in Eq. (2.1) implies that the bosons are hard-core: $n_{r,\eta} \equiv b_{r,\eta}^\dagger b_{r,\eta} = 0, 1$.

Any dimer Hamiltonian has a bosonic representation; in particular, the RK Hamiltonian can be written as

$$H_D = \sum_r \left\{ -J b_{r,1}^\dagger b_{r+e_2,1}^\dagger b_{r,2} b_{r+e_1,2} + (1 \leftrightarrow 2) \right. \\ \left. + V b_{r,1}^\dagger b_{r,1} b_{r+e_2,1}^\dagger b_{r+e_2,1} + (1 \leftrightarrow 2) \right\}. \quad (2.2)$$

To generalise this construction to a large- S formulation, we keep the same Hilbert space as before and replace Eq. (2.1) with the constraint

$$\Pi_r \equiv \sum_{\ell \in \nu_r} b_\ell^\dagger b_\ell - S = 0 \quad (2.3)$$

without changing the Hamiltonian (2.2).

B. Path integral formulation and Gaussian approximation

In what follows, it is convenient to use the radial gauge for the bosonic fields in the path integral formulation of the model:

$$b_{r,\eta} = \sqrt{\rho_\eta(r + e_\eta/2)} \exp \left[i\Phi_\eta(r + e_\eta/2) \right] \quad (2.4) \\ \equiv \sqrt{\frac{S}{z} + \delta\rho_\eta(r + e_\eta/2)} \exp \left[i\Phi_\eta(r + e_\eta/2) \right],$$

where z is the lattice coordination number; for the square lattice, $z = 4$. For later convenience, we think of $\rho_\eta(r + e_\eta/2)$ and $\Phi_\eta(r + e_\eta/2)$ as functions defined on bond midpoints. The RK Hamiltonian is then given by

$$\begin{aligned}
H_D = \sum_r \{ & -2J \sqrt{\rho_1(r+e_1/2)\rho_2(r+e_1+e_2/2)\rho_1(r+e_2+e_1/2)\rho_2(r+e_2/2)} \\
& \times \cos[\Phi_1(r+e_1/2) - \Phi_2(r+e_1+e_2/2) + \Phi_1(r+e_2+e_1/2) - \Phi_2(r+e_2/2)] \\
& + V\rho_1(r+e_1/2)\rho_1(r+e_2+e_1/2) + V\rho_2(r+e_2/2)\rho_2(r+e_1+e_2/2)\}, \quad (2.5)
\end{aligned}$$

and the constraint in Eq. (2.3) can be written as

$$\sum_{\eta} [\delta\rho_{\eta}(r+e_{\eta}/2) + \delta\rho_{\eta}(r-e_{\eta}/2)] = 0. \quad (2.6)$$

We now introduce the Fourier decomposition

$$\delta\rho_{\eta}(r+e_{\eta}/2) = \frac{1}{\sqrt{N}} \sum_k \delta\rho_{\eta}(k) \exp[-ik(r+e_{\eta}/2)], \quad (2.7)$$

$$\Phi_{\eta}(r+e_{\eta}/2) = \frac{1}{\sqrt{N}} \sum_k \Phi_{\eta}(k) \exp[-ik(r+e_{\eta}/2)], \quad (2.8)$$

where $k(r+e_{\eta}/2) \equiv \vec{k} \cdot (\vec{r} + \vec{e}_{\eta}/2)$ for brevity and N is the number of lattice sites. In these terms, the constraint can be written as

$$\sum_{\eta} \cos(ke_{\eta}/2) \delta\rho_{\eta}(k) = 0. \quad (2.9)$$

It will be useful in the following to introduce the shorthand notation $c_{\eta} = \cos(ke_{\eta}/2)$ and $s_{\eta} = \sin(ke_{\eta}/2)$.

The constraint clearly imposes a relation between the two field variables $\delta\rho_1(k)$ and $\delta\rho_2(k)$. The same conclusion can be readily drawn about the fields Φ_{μ} once we notice that the Hamiltonian depends only on the specific combination of them that appears in the argument of the cosine term in Eq. (2.5):

$$\begin{aligned}
\tilde{\phi}(r) \equiv & \Phi_1(r+e_1/2) - \Phi_2(r+e_1+e_2/2) \\
& + \Phi_1(r+e_2+e_1/2) - \Phi_2(r+e_2/2), \quad (2.10)
\end{aligned}$$

whose Fourier transform is

$$\tilde{\phi}(k) = e^{-ik(e_1+e_2)/2} 2[c_2\Phi_1(k) - c_1\Phi_2(k)]. \quad (2.11)$$

Note that the cosine function depends only on powers of $\phi(r)^2$ and therefore phase factors in $\tilde{\phi}(k)$ are immaterial, and we de-

fine for convenience

$$\begin{aligned}
\phi(k) & \equiv e^{ik(e_1+e_2)/2} \tilde{\phi}(k) \\
& = 2[c_2\Phi_1(k) - c_1\Phi_2(k)] \equiv \mathcal{Z}_{\eta}\Phi_{\eta}, \quad (2.12)
\end{aligned}$$

where $\mathcal{Z}_{\eta} = (2c_2, -2c_1)$. In real space, this amounts to introducing a $\phi(r)$ living on the centres of the plaquettes rather than a corner.

Notice that the constraints on $\delta\rho_{\eta}$ and on Φ_{η} are in fact two sides of the same coin – indeed, conjugate variables come in pairs, so their numbers have to be the same. In our case, one can easily verify that imposing one of them implies the other. This is a consequence of how the RK Hamiltonian is designed: the plaquette-flipping term inherently preserves the number of dimers at each vertex; and vice versa, if one imposes the hard core dimer constraint, then any kinetic contribution in the Hamiltonian is projected onto a combination of loop updates, of which the plaquette-flipping term is an example.

To make further progress in the path integral formulation, we shall expand the action to quadratic order in $\phi(r, \tau) \simeq 2n\pi$, $n \in \mathbb{Z}$, and $\delta\rho_{r,\mu} \ll 1$. Firstly, it is convenient to rewrite $\cos(\phi) = 1 - [1 - \cos(\phi)]$ and notice that the term in square brackets contains only quadratic and higher-order contributions. Therefore, the square root in the second term of

$$\sqrt{\rho\rho\rho\rho} \cos(\phi) = \sqrt{\rho\rho\rho\rho} - \sqrt{\rho\rho\rho\rho} [1 - \cos(\phi)], \quad (2.13)$$

needs to be expanded only to leading order in S : $\sqrt{\rho\rho\rho\rho} \simeq S^2/16$. Upon expanding the first term, one obtains both linear and quadratic terms in $\delta\rho_{\eta}(r+e_{\eta}/2)$. However, one can readily convince oneself that the linear terms vanish upon summing over r because of the dimer constraint (2.6). The same is true for the linear contributions due to the terms multiplying V in Eq. (2.5), leading to the following contributions to quadratic order:

$$\begin{aligned}
\sqrt{\rho\rho\rho\rho} \simeq & \frac{S^2}{16} + \frac{1}{4} [\delta\rho_1(r+e_1/2)\delta\rho_2(r+e_1+e_2/2) + \delta\rho_1(r+e_1/2)\delta\rho_1(r+e_2+e_1/2) \\
& + \delta\rho_1(r+e_1/2)\delta\rho_2(r+e_2/2) + \delta\rho_2(r+e_1+e_2/2)\delta\rho_1(r+e_2+e_1/2) \\
& + \delta\rho_2(r+e_1+e_2/2)\delta\rho_2(r+e_2/2) + \delta\rho_1(r+e_2+e_1/2)\delta\rho_2(r+e_2/2)] \quad (2.14)
\end{aligned}$$

$$\begin{aligned}
& - \frac{1}{8} [\delta\rho_1(r+e_1/2)^2 + \delta\rho_1(r+e_2+e_1/2)^2 + \delta\rho_2(r+e_1+e_2/2)^2 + \delta\rho_2(r+e_2/2)^2] \\
\rho\rho + \rho\rho = & \frac{S^2}{8} + \delta\rho_1(r+e_1/2)\delta\rho_1(r+e_2+e_1/2) + \delta\rho_2(r+e_2/2)\delta\rho_2(r+e_1+e_2/2). \quad (2.15)
\end{aligned}$$

Writing the sum of these terms in Fourier space, we get (for the quadratic contributions only):

$$\begin{aligned}
& -Jc_1c_2 [\delta\rho_1(k)\delta\rho_2(-k) + \delta\rho_2(k)\delta\rho_1(-k)] \\
& + [(2V - J)c_2^2 + (J - V)] \delta\rho_1(k)\delta\rho_1(-k) \\
& + [(2V - J)c_1^2 + (J - V)] \delta\rho_2(k)\delta\rho_2(-k). \quad (2.16)
\end{aligned}$$

The dynamics of the model is generated by the standard bosonic Berry phase $\sum_n \bar{b}_n \partial_\tau b_n$. In the radial representation (2.4), this gives rise to the term $\sum_n i \delta\rho_n \partial_\tau \Phi_n$, as well as total derivative terms that do not contribute to the action. Altogether, we obtain

$$\begin{aligned}
S &= \int d\tau \sum_{k,\mu} i \delta\rho_\mu(k, \tau) \partial_\tau \Phi_\mu(-k, \tau) \\
&+ \int d\tau \sum_r \frac{JS^2}{8} [1 - \cos(\phi(r, \tau))] \\
&+ \int d\tau \sum_{k,\mu,\nu} \frac{\mathcal{D}_{\mu\nu}(k)}{2} \delta\rho_\mu(k, \tau) \delta\rho_\nu(-k, \tau), \quad (2.17)
\end{aligned}$$

where

$$\mathcal{D}_{\mu\nu} = 2 \begin{pmatrix} J - V + (2V - J)c_2^2 & -Jc_1c_2 \\ -Jc_1c_2 & J - V + (2V - J)c_1^2 \end{pmatrix}.$$

To proceed further, we can either resolve the constraint explicitly, or keep it implicit. The former allows to relate directly with the customary height field representation for the QDM on the square lattice; the latter is more concise and will be useful to reduce the algebra and obtain analytic results for three dimensional models in Secs. III and VI. For this reason, we present them both in the following sections.

C. Implicit constraint

Let us consider a given cosine minimum at first, and assume $\phi(r, \tau) \ll 1$. (We shall discuss the effect of instantons later in Sec. IID 2.) The middle term in Eq. (2.17) then reduces to

$$\sum_r \frac{JS^2}{16} \phi^2(r, \tau) = \sum_k \frac{JS^2}{16} \mathcal{Z}_\mu \mathcal{Z}_\nu \Phi_\mu(k, \tau) \Phi_\nu(-k, \tau). \quad (2.18)$$

After integrating the first term in Eq. (2.17) by parts in τ , one can integrate the fields Φ_μ out and obtain an action only in terms of the fields $\delta\rho_\mu$:

$$\begin{aligned}
S &= \frac{1}{2} \int d\tau \sum_k \left[(\mathcal{M}^{-1})_{\mu\nu} \partial_\tau \delta\rho_\mu(k, \tau) \partial_\tau \delta\rho_\nu(-k, \tau) \right. \\
&\quad \left. + \mathcal{D}_{\mu\nu}(k) \delta\rho_\mu(k, \tau) \delta\rho_\nu(-k, \tau) \right], \quad (2.19)
\end{aligned}$$

where we define $\mathcal{M} \equiv JS^2 \mathcal{Z} \mathcal{Z}^T / 8$ for convenience. One can now readily obtain the dispersion by computing the eigenvalues of the matrix $\mathcal{M}\mathcal{D}$.

This approach gives us two modes while we know that the physical system is constrained to only one real scalar field. Fortunately, Eq. (2.9) states that $\sum_\mu \mathcal{Z}_\mu \delta\rho_\mu(k) = 0$. Therefore,

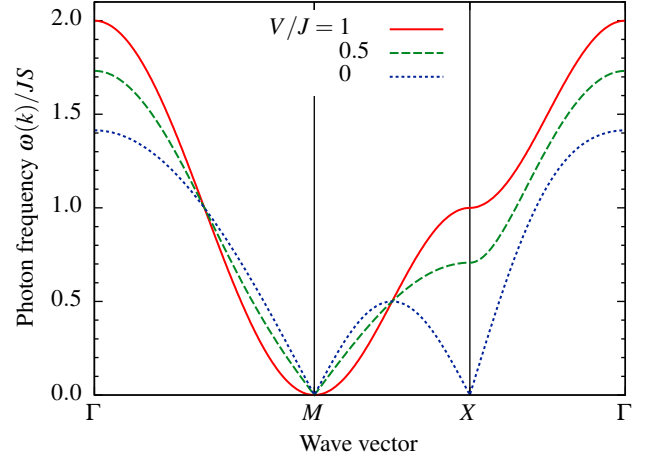


FIG. 2. Photon dispersion relation of the large- S QDM on the square lattice. The spectrum is gapless at the $M = (\pi, \pi)$ point for all values of V/J ; near this point, the dispersion is quadratic at the RK point, and linear away from it. Another minimum forms at the $X = (\pi, 0)$ points for lower V : this drives an ordering transition at $V = 0$.

one of the two eigenvalues of $\mathcal{M}\mathcal{D}$ corresponds to an unphysical mode and vanishes, whereas the other (finite) eigenvalue corresponds to the physical dispersion of the system,

$$\omega^2 = JS^2 [(2V - J)(c_1^4 + c_2^4) + (J - V)(c_1^2 + c_2^2) + 2Jc_1^2c_2^2]. \quad (2.20)$$

This dispersion is plotted for three values of V/J in Fig. 2. It is interesting to note that the dispersion vanishes at (π, π) and symmetry related points for all values of J and V . An instability develops for $V > J$ when the dispersion becomes negative near the (π, π) point (not shown). As we lower the value of V , secondary minima appear at $(\pi, 0)$ and related points in the Brillouin zone, and they drive the system through an instability for $V < 0$ which leads to (plaquette) dimer ordering at these wave vectors.

D. Explicit constraint

The implicit approach in Sec. IIC allows us to arrive at the dispersion of the system with minimal algebra, but it does not produce an action in terms of the physical degree of freedom only. In order to achieve this, we need to resolve the constraint explicitly. A convenient way to do so is to look for a conjugate field $h(k)$ such that the Berry phase in the path integral can be written as $ih(k)\partial_\tau\phi(-k)$:

$$h(k)\partial_\tau\phi(-k) = \sum_\eta \delta\rho_\eta(k)\partial_\tau\Phi_\eta(-k). \quad (2.21)$$

Substituting the expression for $\phi(k)$, Eq. (2.12), into the equation above, we obtain

$$\delta\rho_1(k) = 2c_2 h(k), \quad \delta\rho_2(k) = -2c_1 h(k). \quad (2.22)$$

One can then straightforwardly verify that introducing the field $h(k)$ automatically resolves the constraint:

$$\sum_{\eta} c_{\eta} \delta \rho_{\eta} = 2(c_1 c_2 - c_2 c_1) h(k) = 0. \quad (2.23)$$

Once again, this result should not come as a surprise. It is a reflection, at a field-theoretic level, of the fact that the plaquette terms in the Hamiltonian respect the dimer constraint. Therefore, if the field theory is built from plaquette kinetic terms only, then the constraint is implied.

We are thus in the position to write the full large- S action for the system, including both the Berry phase and Hamiltonian contributions, in terms of the fields $h(k)$ and $\phi(k)$ only. Adding more complicated ring exchange type terms to the RK Hamiltonian does not invalidate this conclusion, as the phase in each ring exchange term may be written as a sum of phases over single plaquettes. Substituting the expressions of $\delta \rho_{\eta}(k)$ in terms of $h(k)$, and ignoring trivial constants, we obtain the action:

$$S = \int d\tau \sum_r \left\{ i h(r, \tau) \partial_{\tau} \phi(r, \tau) + \frac{JS^2}{8} [1 - \cos(\phi(r, \tau))] \right\} + \int d\tau \sum_k \frac{\mathcal{D}_0(k)}{2} h(k, \tau) h(-k, \tau) \quad (2.24)$$

where

$$\mathcal{D}_0(k) = 8[(2V - J)(c_1^4 + c_2^4) + (J - V)(c_1^2 + c_2^2) + 2Jc_1^2 c_2^2]. \quad (2.25)$$

1. Action without instantons

Ignoring for the time being the contribution to the action due to instantons between different minima of the cosine term, we can expand about one given minimum and integrate over ϕ to arrive at

$$S = \frac{1}{2} \int d\tau \sum_k \left[\frac{8}{JS^2} \partial_{\tau} h(k, \tau) \partial_{\tau} h(-k, \tau) + \mathcal{D}_0(k) h(k, \tau) h(-k, \tau) \right]. \quad (2.26)$$

One can easily see that the dispersion is indeed the same as in Eq. (2.20).

Expanding \mathcal{D}_0 about its minimum at (π, π) ,

$$\mathcal{D}_0[(\pi, \pi) + (k_x, k_y)] \simeq 2(J - V)(k_x^2 + k_y^2) + \left[\frac{7V}{6} - \frac{2J}{3} \right] (k_x^4 + k_y^4) + Jk_x^2 k_y^2,$$

we obtain the action

$$S = \frac{1}{2} \int d\tau d^2r \left\{ \frac{8}{JS^2} (\partial_{\tau} h)^2 + 2(J - V)(\nabla h)^2 + \frac{7V - 4J}{6} h (\partial_x^4 + \partial_y^4) h + Jh (\partial_x^2 \partial_y^2) h \right\} + \dots \quad (2.27)$$

At the RK point, the $(\nabla h)^2$ term vanishes and the terms with quartic derivatives add up to

$$\frac{J}{2} (\nabla^2 h)^2, \quad (2.28)$$

yielding the spectrum $\omega = k^2/2m$ with $m = 2/JS$. We note that the known value at the RK point for $S = 1$ (and $J = V = 1$) in this normalisation is $m = 9/\pi$ (corresponding to $K = \pi/18$ in Refs. 5 and 12), which can be obtained exactly from the ground-state wave function of the QDM, available only at the RK point). This shows that, expanding to quadratic order, our estimate is within 40% accuracy. We note that such a discrepancy at quadratic order in a large- S expansion is consistent for instance with similar results obtained in Ref. 16 for quantum spin ice. Our results can be improved by going to higher orders, and – more importantly with respect to earlier work on field theories for quantum dimer models – their validity is not limited to the fine tuned RK point.

2. Instantons

We will now incorporate the instanton effects which, as we shall demonstrate, always generate a mass for the photons for $V < J$, as it generally happens in compact electrodynamics. To this end, we are going to integrate out the field $\phi(r, \tau)$ taking into account the fact that the action is periodic in it.

Firstly, we proceed by the standard Villain approach and replace

$$1 - \cos \phi \rightarrow \frac{1}{2} \left[\phi - 2\pi \sum_j q_j \theta(\tau - \tau_j) \right]^2, \quad (2.29)$$

where the $q_j = q(r_j, \tau_j)$ are integers representing instanton events, and $\theta(\tau)$ is the Heaviside step function. By integrating over ϕ and h , we obtain the following action:

$$S = \frac{(2\pi)^2}{2} \sum_{j,k} q(r_j, \tau_j) G_{qq}(r_j - r_k; \tau_j - \tau_k) q(r_k, \tau_k) G_{qq}(k, \omega) = \left[\omega^2/M + (\rho_2 k^2 + \rho_4 k^4) \right]^{-1}, \quad (2.30)$$

where $M = JS^2/8$ and we introduced the symbolic terms $\rho_2 k^2$ and $\rho_4 k^4$ to represent the quadratic and quartic derivative terms in the action: $\mathcal{D}_0(k) \simeq \rho_2 k^2 + \rho_4 k^4 + \dots$. The resulting partition function is that of a Coulomb gas of charges $q = \pm 1, \pm 2, \dots$, where the fugacity of charge q is given by $I = \exp(-q^2 \mathcal{S}_0)$ and \mathcal{S}_0 is the contribution to the action from a single instanton with $q = 1$:

$$\mathcal{S}_0 = \frac{1}{4\pi} \int \frac{d\omega d^2k}{\omega^2/M + (\rho_2 k^2 + \rho_4 k^4)} \simeq \frac{\pi S}{8} \sqrt{\frac{J}{2\rho_4}} \ln(\rho_4/\rho_2), \quad (2.31)$$

and hence

$$I = (\rho_2/\rho_4)^{q^2 \pi S/8}, \quad (2.32)$$

where we performed the calculations with the RK form of the quartic term and substituted $\rho_4 = J/2$ for simplicity.

Since I is a rapidly decaying function of the instanton charge, we can restrict our consideration to the gas of charges $q = \pm 1$. Following Polyakov [17], we approximate the partition function of the Coulomb gas (2.30) as the one of the

sine-Gordon model with action (2.27) augmented by the term

$$\delta S = -2\mu I \int d\tau \sum_r \cos(2\pi h), \quad (2.33)$$

where $\mu d\tau$ is the preexponential part of the instanton measure (see Appendix A); at the RK point, $2\mu = JS^{3/2} \sqrt{\pi}/2$. The presence of this term makes the excitations massive:

$$\omega^2 = c^2 k^2 + m^2, \quad m^2 = 8\pi^2 M\mu I. \quad (2.34)$$

As we see from (2.32), this mass vanishes at the RK point.

At finite temperatures, instantons interact logarithmically:

$$E = -\frac{2\pi T^2}{\rho_2} \sum_{j < k} q_j q_k \ln \left(\frac{|r_j - r_k|}{r_0} \right), \quad (2.35)$$

where $r_0^2 = \rho_4/\rho_2$. The corresponding contribution to the free energy density

$$\delta F \propto q^2 I_q \int \frac{d^2 r}{r^{d_q}}, \quad d_q = 2\pi q^2 T/\rho_2, \quad (2.36)$$

diverges at small T . The contribution of the static fluctuations of h is encoded in the free energy functional

$$F = \int d^2 r \left[\frac{\rho_2}{2} (\nabla h)^2 + \frac{\rho_4}{2} (\nabla^2 h)^2 - 2\mu I \cos(2\pi h) \right]. \quad (2.37)$$

The scaling dimension d_1 of the cosine term is given by (2.36). The critical temperature above which the cosine term is irrelevant is determined by the condition $d_1 = 2$:

$$T_c = \rho_2/\pi. \quad (2.38)$$

Above T_c , we have a critical phase; below it, the correlation length of the h field is finite:

$$\xi \sim r_0 (\mu I/T_c)^{-1/(2-d_1)} \quad (2.39)$$

This corresponds to melting the valence bond crystal. As it is typical for 2D crystals, it melts via a Berezinskii–Kosterlitz–Thouless transition.

We finally take a moment to comment on the difference between our result and the one obtained in Ref. 18, which in fact addresses a somewhat different problem. In Ref. 18 the authors considered equal time correlations at the RK point. The remarkable property of this point is that the ground-state wave function can be represented as a path integral with a Gaussian action. It was argued that the periodicity of the height field generates the irrelevant perturbation $\cos(2\pi h)$. Here, we obtained a formally equivalent perturbation (2.33) also away from the RK point; however, the prefactor of the cosine term in our case vanishes precisely at the RK point.

E. Large- S phase diagram

As $S \rightarrow \infty$, zero point fluctuations of any soft modes are negligible, and ρ and Φ can be treated as commuting, classical

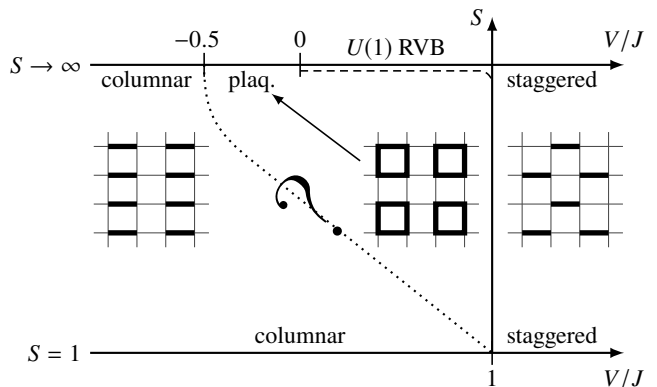


FIG. 3. Phase diagram of the square lattice quantum dimer model at $S = \infty$ (this work) and $S = 1$ [19–26].

variables. The ground state energy of the system in this limit is therefore given by classical minimisation of the Hamiltonian (2.5). Since $\sqrt{\rho\rho\rho\rho} \geq 0$ always, the Φ in such an optimal state satisfy $\cos(\Phi_1 - \Phi_2 + \Phi_3 - \Phi_4) = 1$ which is achieved, for instance, by setting $\Phi \equiv 0$.

Finding the optimal values of ρ in full generality is more difficult. However, one can always compare the ground state energies of phases suggested in the literature, or develop a variational ansatz that captures several such phases. In the case of the square lattice, we considered states in which ρ is constant within each set of bonds populated in the four columnar ordered states. Such an ansatz can capture columnar and plaquette ordered states as well as the RVB liquid phase.

Comparing the ground state energies of these phases yields the $S \rightarrow \infty$ phase diagram shown in Fig. 3. As expected, the ground state is staggered for $V > J$ and columnar at $V \rightarrow -\infty$. At intermediate V/J , we see a plaquette ordered phase as well as an extended $U(1)$ RVB liquid, with phase boundaries corresponding to the instabilities shown in Fig. 2. The latter is unstable at finite S due to instanton effects, as discussed above. The fate of the plaquette phase is, however, less clear: since it is ordered, instantons are unlikely to substantially affect its stability, and so the evolution of the columnar–plaquette phase boundary must mostly depend on lattice effects. It may well be possible that the plaquette order survives at $S > 1$ and has a proximity effect near the RK point even at $S = 1$. This could explain why numerical simulations of the square lattice dimer model struggle to establish its true ground state in this regime [19–26].

III. CUBIC LATTICE

The calculations for other lattices are straightforward generalisations of the square lattice case, with minimal but informative modifications. We begin with the cubic lattice, where we have the three lattice vectors $e_\eta = \hat{x}, \hat{y}, \hat{z}$. The correspond-

ing RK Hamiltonian can be written as:

$$H_D = \sum_r \left\{ -J b_{r,1}^\dagger b_{r+e_2,1}^\dagger b_{r,2} b_{r+e_1,2} + (1 \leftrightarrow 2) \right. \\ \left. + V b_{r,1}^\dagger b_{r,1} b_{r+e_2,1}^\dagger b_{r+e_2,1} + (1 \leftrightarrow 2) \right\} \\ + (12) \leftrightarrow (13) \leftrightarrow (23), \quad (3.1)$$

subject to the equivalent large- S constraint

$$\Pi_r \equiv \sum_{l \in \nu_r} b_l^\dagger b_l - S = 0. \quad (3.2)$$

Using the radial gauge expression (2.4) for the bosonic field with $z = 6$, this constraint can be written as in (2.6), which in Fourier space reduces to

$$\sum_\eta c_\eta \delta \rho_\eta(k) = 0. \quad (3.3)$$

Contrary to the case of the square lattice, we have now three fields $\delta \rho_\eta$ and one constraint, leaving two independent field

variables. The Hamiltonian is made of three terms equivalent to the square lattice Eq. (2.5), upon replacing (12) \leftrightarrow (13) \leftrightarrow (23).

As we did for the square lattice QDM, we derive here the resulting field theory to quadratic order. The calculation is similar to the one carried out in Sec. II C, keeping the constraints implicit. It is also possible to explicitly resolve the constraints and obtain an action in terms of two independent real scalar fields, as in Sec. II D, but for brevity, we omit the details of the calculation and only present the final result at the end of this section.

The terms in the cubic Hamiltonian are equivalent to combining the square lattice terms for the (12), (13), and (23) components, see Eqs. (2.13), (2.14), and (2.15), up to a factor of 4/9 due to the fraction $S/6$ replacing $S/4$ in Eq. (2.4):

$$S = \int d\tau \left\{ \sum_{k,\mu} i \delta \rho_\mu(k) \partial_\tau \Phi_\mu(-k) + \frac{JS^2}{18} \sum_{r,\mu} [1 - \cos(\phi_\mu(r, \tau))] + \sum_{k,\mu,\nu} \frac{\mathcal{D}_{\mu\nu}}{2} \delta \rho_\mu(k) \delta \rho_\nu(-k) \right\}, \quad (3.4)$$

where

$$\mathcal{D} = 2 \begin{pmatrix} 2(J-V) + (2V-J)(c_2^2 + c_3^2) & -Jc_1c_2 & -Jc_1c_3 \\ -Jc_1c_2 & 2(J-V) + (2V-J)(c_1^2 + c_3^2) & -Jc_2c_3 \\ -Jc_1c_3 & -Jc_2c_3 & 2(J-V) + (2V-J)(c_1^2 + c_2^2) \end{pmatrix}, \quad (3.5)$$

and we labelled ϕ_μ the argument of the cosine term involving the phase fields Φ_ν with $\nu \neq \mu$.

A. Action without instantons

When we expand about one given minimum,

$$\frac{JS^2}{18} \sum_{\mu=1,2,3} [1 - \cos(\phi_\mu(r, \tau))] \simeq \frac{JS^2}{36} \sum_{\mu=1,2,3} \phi_\mu(r, \tau)^2, \quad (3.6)$$

we see that integrating out the fields ϕ_μ requires some care, since they are not all independent of one another.

Following the same steps as for the square lattice dimer model, it is convenient to introduce in Fourier space the fields

$$\begin{aligned} \phi_1(k) &\equiv e^{ik(e_2+e_3)/2} \tilde{\phi}_1(k) = 2[c_3\Phi_2(k) - c_2\Phi_3(k)] \\ \phi_2(k) &\equiv e^{ik(e_3+e_1)/2} \tilde{\phi}_2(k) = 2[c_1\Phi_3(k) - c_3\Phi_1(k)] \\ \phi_3(k) &\equiv e^{ik(e_1+e_2)/2} \tilde{\phi}_3(k) = 2[c_2\Phi_1(k) - c_1\Phi_2(k)]. \end{aligned} \quad (3.7)$$

These are most conveniently expressed as $\phi_\mu = \mathcal{Z}_{\mu\nu} \Phi_\nu$, where $\mathcal{Z}_{\mu\nu} = 2\varepsilon_{\mu\nu\lambda} c_\lambda$ ($\varepsilon_{\mu\nu\lambda}$ is the fully antisymmetric tensor and summation is implied).

Notice that \mathcal{Z} is a nonzero traceless antisymmetric matrix. It has one zero eigenvalue, $\sum_\nu \mathcal{Z}_{\mu\nu} c_\nu = 0$, and the other two must be non-vanishing and opposite, $\pm\zeta$:

$$2\zeta^2 = \text{tr} \mathcal{Z}^2 = -2(c_1^2 + c_2^2 + c_3^2), \quad \zeta = i \sqrt{c_1^2 + c_2^2 + c_3^2}. \quad (3.8)$$

The two non-vanishing eigenvectors define the physical space, and the null one is the gauge degree of freedom. One can therefore construct a projector onto the physical space as $-\mathcal{Z}^2/(c_1^2 + c_2^2 + c_3^2)$.

The cosine term in the Hamiltonian reduces to

$$\begin{aligned} \frac{JS^2}{36} \sum_\mu \phi_\mu(k) \phi_\mu(-k) &= \frac{JS^2}{36} \phi^T(k) \phi(-k) \\ &= \frac{JS^2}{36} \Phi^T(k) \mathcal{Z}^T(k) \mathcal{Z}(-k) \Phi(-k) \\ &= -\frac{JS^2}{36} \Phi^T(k) \mathcal{Z}^2(k) \Phi(-k) \\ &= \sum_{\mu\nu} \frac{\mathcal{M}_{\mu\nu}}{2} \Phi_\mu(k) \Phi_\nu(-k), \end{aligned} \quad (3.9)$$

where we used the fact that $\mathcal{Z}(-k) = \mathcal{Z}(k)$ and $\mathcal{Z}^T = -\mathcal{Z}$,

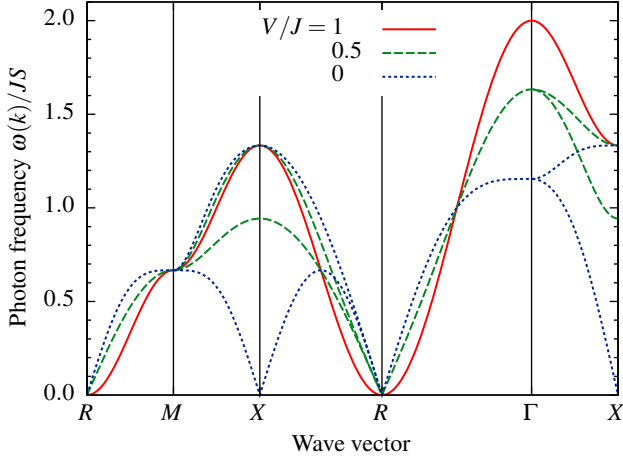


FIG. 4. Photon dispersion relation of the large- S QDM on the cubic lattice. The spectrum is gapless at the $R = (\pi, \pi, \pi)$ point; near this point, the dispersion is quadratic at the RK point and linear away from it. The spectrum has two non-degenerate branches away from the RK point. The lower branch develops minima at the $X = (\pi, 0, 0)$ points for lower values of V , which drives an ordering transition at $V = 0$.

and we defined

$$\begin{aligned} \mathcal{M} &= -\frac{JS^2}{18} \mathcal{Z}^2 \\ &= \frac{2JS^2}{9} \begin{pmatrix} c_2^2 + c_3^2 & -c_1 c_2 & -c_1 c_3 \\ -c_1 c_2 & c_1^2 + c_3^2 & -c_2 c_3 \\ -c_1 c_3 & -c_2 c_3 & c_1^2 + c_2^2 \end{pmatrix}. \end{aligned} \quad (3.10)$$

Integrating out the fields Φ_μ then gives

$$\frac{1}{2} \sum_{\mu, \nu} \mathcal{M}_{\mu\nu}^{-1} \partial_\tau \delta \rho_\mu(k) \partial_\tau \delta \rho_\nu(-k), \quad (3.11)$$

so we can write the full quadratic action without instantons as

$$\mathcal{S} = \frac{1}{2} \int d\tau \sum_{k, \mu, \nu} \left[\mathcal{M}_{\mu\nu}^{-1} \partial_\tau \delta \rho_\mu(k) \partial_\tau \delta \rho_\nu(-k) + \mathcal{D}_{\mu\nu} \delta \rho_\mu(k) \delta \rho_\nu(-k) \right]. \quad (3.12)$$

The dispersion can be obtained from the eigenvalues of $\mathcal{M}\mathcal{D} = -2JS^2\mathcal{Z}^2\mathcal{D}/9$, after projecting out the unphysical modes that do not satisfy the constraint $\sum_\mu c_\mu \delta \rho_\mu = 0$. This could be done formally by adding an infinite Lagrange multiplier, but in fact there is no need to do so because the only unphysical mode is trivially the zero mode of $\mathcal{Z}^2\mathcal{D}$ – as we had previously observed in the square lattice QDM. The two non-vanishing eigenvalues are

$$\begin{aligned} \omega^2 &= \frac{4JS^2}{9} \left\{ J \left[2(c_1^2 + c_2^2 + c_3^2) - (c_1^4 + c_2^4 + c_3^4) \right] \right. \\ &\quad + 2V \left[c_1^4 + c_2^4 + c_3^4 - (c_1^2 + c_2^2 + c_3^2) + c_1^2 c_2^2 + c_1^2 c_3^2 + c_2^2 c_3^2 \right] \\ &\quad \left. \pm 2|J - V| \sqrt{c_1^4 c_2^4 + c_1^4 c_3^4 + c_2^4 c_3^4 - c_1^2 c_2^2 c_3^2 (c_1^2 + c_2^2 + c_3^2)} \right\}. \end{aligned} \quad (3.13)$$

This dispersion is plotted for three values of V/J in Fig. 4. It

is interesting to note that $\omega^2|_{J=V} \propto (c_1^2 + c_2^2 + c_3^2)^2$ and the two bands are degenerate at the RK point, with vanishing minima at (π, π, π) and symmetry related points, and quadratic dispersion around them. Expanding near such minima, we find

$$\omega^2 \simeq \frac{2S^2}{9} J(J - V) k^2, \quad (3.14)$$

where k is the (small) vector distance from the minimum, giving a speed of light

$$c = \frac{S}{3} \sqrt{2J(J - V)}. \quad (3.15)$$

As mentioned earlier, one could have alternatively resolved the constraint explicitly, writing the three fields $\delta \rho_\mu$ in terms of two independent real scalar fields h_a and resolving the corresponding interdependence of the three fields ϕ_μ :

$$c_1 \phi_1 + c_2 \phi_2 + c_3 \phi_3 = 0. \quad (3.16)$$

For instance, one can do so via the relation $\phi_1 = -(c_2/c_1)\phi_2 - (c_3/c_1)\phi_3$ and $\delta \rho_\mu = \sum_a R_{\mu a} h_a$ with

$$R = 2 \begin{pmatrix} c_2 & -c_3 \\ c_1 & 0 \\ 0 & c_1 \end{pmatrix}. \quad (3.17)$$

After a few lines of algebra, one arrives at the action

$$\mathcal{S} = \frac{1}{2} \int d\tau \sum_{k, a, b} \left[\widetilde{\mathcal{M}}_{ab}^{-1} \partial_\tau h_a(k) \partial_\tau h_b(-k) + \widetilde{\mathcal{D}}_{ab} h_a(k) h_b(-k) \right] \quad (3.18)$$

where $\widetilde{\mathcal{D}} = R^T \mathcal{D} R$ and

$$\widetilde{\mathcal{M}} = \frac{JS^2}{18c_1^2} \begin{pmatrix} c_1^2 + c_2^2 & c_2 c_3 \\ c_2 c_3 & c_1^2 + c_3^2 \end{pmatrix}.$$

One can easily verify that the action (3.18) gives indeed the same dispersion as Eq. (3.13).

B. Instantons

The instanton contributions are calculated similarly to the square lattice case, by performing the Villain transformation (2.29) on ϕ_μ in (3.4) and integrating out the smooth fields ϕ_μ, h_μ . The result is a 3D Coulomb gas action for the integer charges q_μ ,

$$\mathcal{S} = \frac{(2\pi)^2}{2} \sum_{\omega, k} \sum_{\mu, \nu} q_\mu(-\omega, -k) \left[\frac{18\omega^2}{JS^2} \mathcal{M}^{-1} + \mathcal{D} \right]_{\mu\nu}^{-1} q_\nu(\omega, k), \quad (3.19)$$

with the standard unscreened long-range Coulomb interaction. However, the constraint (3.16) on the fields ϕ_μ implies the equivalent constraint

$$c_1 q_1 + c_2 q_2 + c_3 q_3 = 0 \quad (3.20)$$

on the instanton configurations $q_\mu(\omega, k)$ allowed in the low-energy sector. In $(3+1)$ dimensions, such instantons are irrelevant and can be safely neglected.

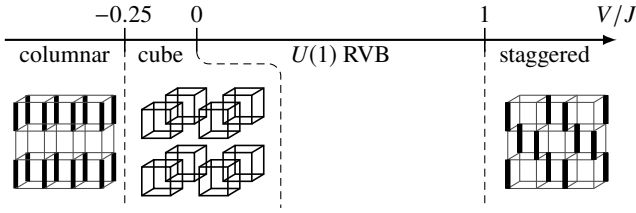


FIG. 5. $S \rightarrow \infty$ phase diagram of the cubic lattice quantum dimer model. (To our knowledge, there are no conclusive studies of the $S = 1$ QDM on the cubic lattice, to which one could compare the large S results of this work.)

C. Large- S phase diagram

Using the method described in Sec. II E, we can obtain the ground state of the QDM Hamiltonian (3.1) in the limit $S \rightarrow \infty$. The results are summarised in Fig. 5. Similarly to the square lattice case, we observe an extended $U(1)$ RVB liquid phase: in three dimensions, this phase is anticipated to survive at $S = 1$. For $V > J$, the photon modes become unstable at the (π, π, π) point, leading to staggered order. Likewise, the instability of the $(\pi, 0, 0)$ points for $V < 0$ drives a transition into an RVB solid phase with isolated, resonating cubes. For $V < -J/4$, this phase gives way to columnar order.

IV. TRIANGULAR LATTICE

It is interesting to consider the case of the triangular lattice QDM immediately after the cubic one. It has sixfold connectivity and is tripartite, and one can view it as a cubic lattice projected along one of the $[111]$ directions. Following the notation in Fig. 6, the solid dots belong to one cubic sublattice, the open circles to the other, and the dotted circles are sites that belong to both cubic sublattices but get projected onto one another. The rhombic plaquettes of the triangular lattice correspond to the three independent faces of a cube, and therefore one can precisely identify flippable plaquettes and plaquette flipping terms between the two models. This projective view allows us to draw a complete correspondence between the two QDMs. Formally, the large- S path integral approach presented in this paper proceeds identically, down to the numerical prefactors, for the triangular and cubic cases and we end up with the same two-component field theory [29], with action given (to quadratic order) by Eq. (3.12) and dispersion given by Eq. (3.13). The correspondence holds only so long as we express the positions and wave vectors formally as r and k , and the basis vectors as e_1, e_2 and e_3 .

To study the triangular lattice QDM, one then needs to substitute $k = (k_x, k_y)$ and a given choice of base vectors, for example $e_1 = (\sqrt{3}, 1)/2$, $e_2 = (-\sqrt{3}, 1)/2$, and $e_3 = (0, -1)$, illustrated in Fig. 6. This is, however, beyond the scope of the present paper. For $S = 1$, we expect a \mathbb{Z}_2 liquid phase to be stable around the RK point [30]; its fate, however, is unclear in the large- S limit. If the description is able to capture it at all, it can only be after accounting for instantons and understanding

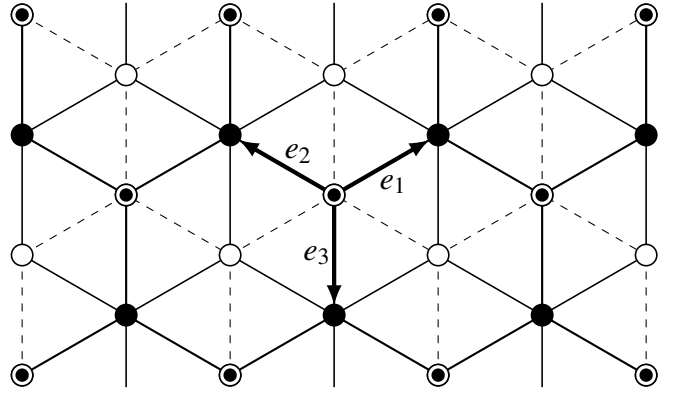


FIG. 6. The triangular lattice illustrating a choice of base vectors $e_{1,2,3}$. Its three sublattices are shown as solid dots, open circles, and dotted circles. Some bonds of the lattice appear as dashed rather than solid lines, in accordance with the correspondence to a projected cubic lattice discussed in the main text.

how their role differs in bipartite and non-bipartite lattices – a task which promises to pose non-trivial challenges.

V. HONEYCOMB LATTICE

In this section, we consider the QDM on the honeycomb lattice, illustrated in Fig. 7, and we present only the approach in which the constraint is resolved explicitly. Contrary to the cases considered so far, the primitive cell of the lattice contains two distinct sites (shown as solid dots and open circles in the figure). With the choice of lattice vectors $e_1 = (\sqrt{3}, 1)/2$, $e_2 = (-\sqrt{3}, 1)/2$, and $e_3 = (0, -1)$ in Fig. 7, we can write the bosonic representation of the Hamiltonian as

$$H_D = \sum_{r \in A} \left\{ -J b_{r,1}^\dagger b_{r+e_1-e_3,2}^\dagger b_{r+e_2-e_3,3}^\dagger \right. \\ \times b_{r+e_1-e_3,3} b_{r+e_2-e_3,1} b_{r,2} + \text{h.c.} \\ \left. + V b_{r,1}^\dagger b_{r,1} b_{r+e_1-e_3,2}^\dagger b_{r+e_1-e_3,2} b_{r+e_2-e_3,3}^\dagger b_{r+e_2-e_3,3} \right. \\ \left. + V b_{r+e_1-e_3,3}^\dagger b_{r+e_1-e_3,3} b_{r+e_2-e_3,1}^\dagger b_{r+e_2-e_3,1} b_{r,2}^\dagger b_{r,2} \right\}. \quad (5.1)$$

One has to write two separate (large- S) constraints, one for each sublattice:

$$\sum_{l \in V_{r \in A}} b_l^\dagger b_l - S = 0, \quad \sum_{l \in V_{r \in B}} b_l^\dagger b_l - S = 0. \quad (5.2)$$

The rest of the calculation follows rather straightforwardly from the square lattice case, barring some added algebraic difficulties, and is presented for completeness in App. B. The argument of the cosine leads us to introduce the field

$$\phi(k) = 2i \left[\Phi_1(k)(s_2 c_3 - s_3 c_2) + \Phi_2(k)(s_3 c_1 - s_1 c_3) \right. \\ \left. + \Phi_3(k)(s_1 c_2 - s_2 c_1) \right]$$

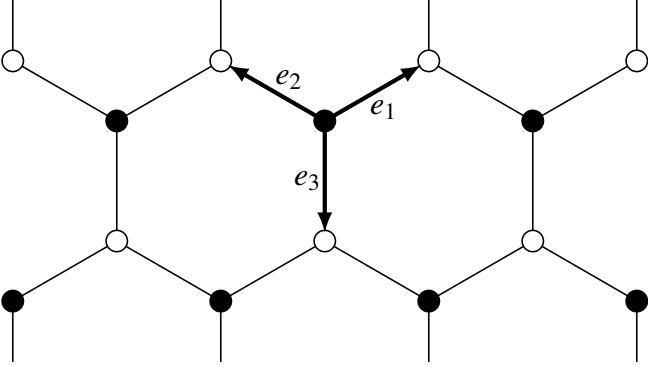


FIG. 7. Honeycomb lattice showing the lattice vectors $e_{1,2,3}$ defined in the text.

and the following convenient resolution of the constraint in terms of a scalar field $h(k)$:

$$\begin{aligned}\delta\rho_1(k) &= -2i(s_2c_3 - s_3c_2)h(k) \\ \delta\rho_2(k) &= -2i(s_3c_1 - s_1c_3)h(k) \\ \delta\rho_3(k) &= -2i(s_1c_2 - s_2c_1)h(k).\end{aligned}\quad (5.3)$$

To quadratic order, one arrives then at the action

$$\begin{aligned}S &= \int d\tau \sum_r \left\{ ih(r, \tau) \partial_\tau \phi(r, \tau) + \frac{2JS^3}{27} [1 - \cos(\phi(r, \tau))] \right\} \\ &+ \int d\tau \sum_k \frac{D(k)}{2} h(k, \tau) h(-k, \tau),\end{aligned}\quad (5.4)$$

where

$$\begin{aligned}D(k) &= \frac{8JS}{3}(s_{12}^4 + s_{23}^4 + s_{31}^4) \\ &- \frac{16JS}{3}(s_{12}s_{23}c_{12}c_{23} + s_{23}s_{31}c_{23}c_{31} + s_{31}s_{12}c_{31}c_{12}) \\ &+ \frac{16VS}{3} \left[s_{12}s_{23}(c_{12}c_{23} - s_{12}s_{23}) \right. \\ &\quad \left. + s_{23}s_{31}(c_{23}c_{31} - s_{23}s_{31}) \right. \\ &\quad \left. + s_{31}s_{12}(c_{31}c_{12} - s_{31}s_{12}) \right],\end{aligned}\quad (5.5)$$

where we introduce for convenience

$$\begin{aligned}s_{\mu\nu} &= \sin[k(e_\mu - e_\nu)/2] = s_\mu c_\nu - s_\nu c_\mu \\ c_{\mu\nu} &= \cos[k(e_\mu - e_\nu)/2] = c_\mu c_\nu + s_\mu s_\nu.\end{aligned}\quad (5.6)$$

Expanding about one given minimum,

$$\frac{2JS^3}{27} [1 - \cos(\phi(r, \tau))] \simeq \frac{JS^3}{27} \phi(r, \tau)^2, \quad (5.7)$$

and integrating over ϕ , we arrive at the action

$$\begin{aligned}S &= \frac{1}{2} \int d\tau \sum_k \left[\frac{27}{2JS^3} \partial_\tau h(k, \tau) \partial_\tau h(-k, \tau) \right. \\ &\quad \left. + D(k)h(k, \tau)h(-k, \tau) \right],\end{aligned}\quad (5.8)$$

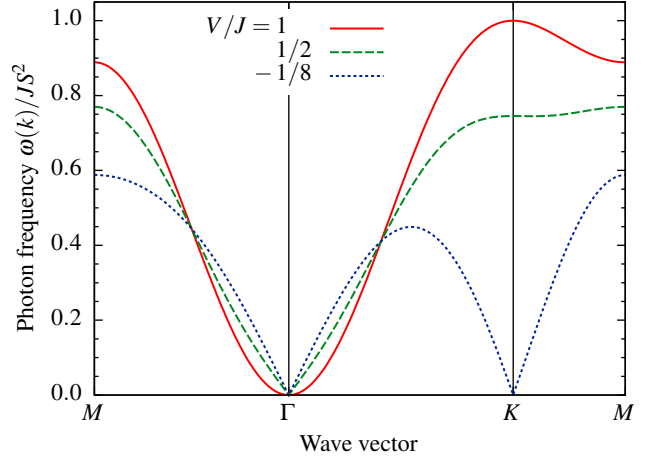


FIG. 8. Photon dispersion relation of the large- S QDM on the honeycomb lattice. The spectrum is gapless at the Γ point. Another minimum develops for small V at the K points; however, a plaquette ordering transition occurs before this minimum would become unstable.

and the corresponding dispersion $\omega^2(k) = 2JS^3 D(k)/27$. This dispersion is plotted for three values of V/J in Fig. 8. It is gapless at the Γ point for all values of J and V . An instability develops for $V > J$ whereby ω^2 becomes negative for small k . For $V \lesssim J$, the long-wavelength dispersion is linear:

$$\omega \simeq \frac{\sqrt{2J(J-V)}S^2}{3}k. \quad (5.9)$$

As the value of V is lowered, secondary minima appear at the K points in the Brillouin zone which drive the system through an instability for $V < -J/8$.

Expanding $D(k)$ about its minimum at $\Gamma = (0, 0)$,

$$\begin{aligned}D[(k_x, k_y)] &\simeq 3S(J-V)(k_x^2 + k_y^2) \\ &+ \frac{9S}{16}(7V-J)(k_x^4 + k_y^4 + 2k_x^2k_y^2),\end{aligned}$$

we obtain the action:

$$\begin{aligned}S &= \frac{1}{2} \int d\tau d^2r \left[\frac{27}{2JS^3} (\partial_\tau h)^2 + 3S(J-V)(\nabla h)^2 \right. \\ &\quad \left. + \frac{9S}{16}(7V-J)(\nabla^2 h)^2 \right] + \dots\end{aligned}\quad (5.10)$$

Contrary to the square lattice QDM, see Eq. (2.27), we find that rotational symmetry is preserved near the band minimum of the honeycomb lattice QDM for $J \neq V$, at least up to quartic order. This is expected, since the discrete symmetry of the lattice upon $2\pi/3$ rotations implies that the first symmetry-breaking term allowed in the action must be of sixth order in k .

The ground state of the $S \rightarrow \infty$ model was also obtained as a function of V/J by comparing the energy of several ordered and resonating phases suggested in the literature [31, 32] under the Hamiltonian (5.1). The resulting phase diagram is

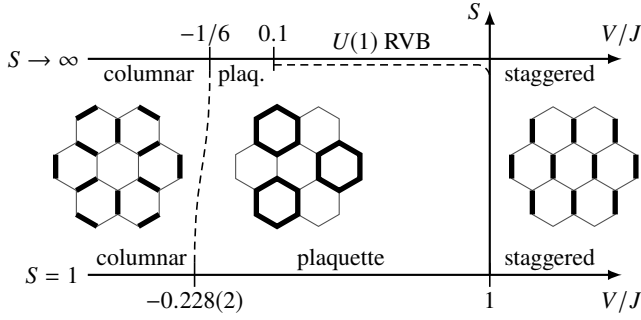


FIG. 9. Phase diagram of the honeycomb lattice quantum dimer model at $S = \infty$ (this work) and $S = 1$ [32].

shown in Fig. 9, together with the $S = 1$ phase diagram obtained in Ref. [32]. As in the previous cases, the large- S phase diagram predicts a columnar ordered, a plaquette ordered, an RVB liquid, and a staggered ordered phase, which are also sketched in Fig. 9. It is interesting to note that the RVB liquid phase instability for $V < J$ occurs below the RVB–plaquette transition point (cf. Figs. 8 and 9); this suggests that the latter may in fact be a first order transition. At finite S , instantons are expected to gap out the $U(1)$ liquid phase in two dimensions, leading to its immediate collapse, see Sec. IID 2. The other three phases are all observed at $S = 1$ with critical V/J similar to the large- S result.

VI. DIAMOND LATTICE

The diamond lattice is composed of two interpenetrating face centred cubic (fcc) lattices, as shown in Fig. 10. Sublattice A is connected to sublattice B by the vectors

$$\begin{aligned} e_1 &= \frac{1}{\sqrt{3}}(1, 1, 1) & e_2 &= \frac{1}{\sqrt{3}}(1, -1, -1) \\ e_3 &= \frac{1}{\sqrt{3}}(-1, 1, -1) & e_4 &= \frac{1}{\sqrt{3}}(-1, -1, 1), \end{aligned} \quad (6.1)$$

which we chose to define the unit length in the system. Notice that $\sum_{\mu} e_{\mu} = 0$. The lattice is fourfold coordinated and the smallest lattice loop over which a dimer move can take place is a hexagon. Each hexagonal plaquette involves lattice bonds of three out of the four types, and therefore there are four inequivalent plaquette terms, involving respectively $\mu = 1, 2, 3, \mu = 1, 2, 4, \mu = 1, 3, 4$, and $\mu = 2, 3, 4$.

The QDM Hamiltonian is the sum of four copies of the honeycomb lattice Hamiltonian (5.1) and we refrain from writing it here explicitly for convenience (see Sec. V and App. B). Expressing the bosonic operators in the radial gauge (2.4) and

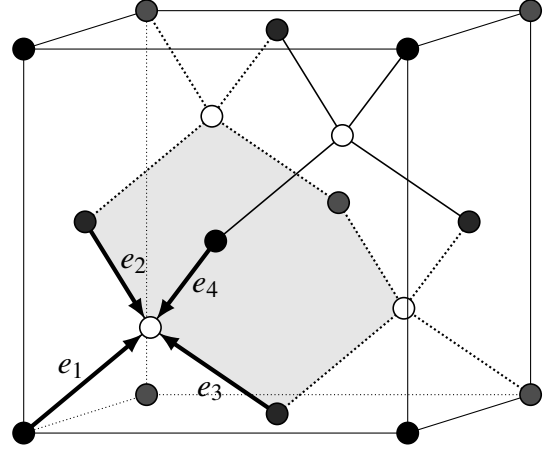


FIG. 10. Unit cell of the diamond lattice showing the lattice vectors $e_{1,\dots,4}$ introduced in the text. The two interpenetrating fcc lattices are shown as solid and open dots, respectively. A hexagonal plaquette is shown shaded by way of example.

expanding to quadratic order in $\delta\rho$ leads to the action

$$\begin{aligned} \mathcal{S} &= \int d\tau \sum_{k,\mu} i\delta\rho_{\mu}(k, \tau) \partial_{\tau} \Phi_{\mu}(-k, \tau) \\ &+ \int d\tau \sum_{r,\alpha} \frac{JS^2}{8} [1 - \cos(\phi_{\alpha}(r, \tau))] \\ &+ \int d\tau \sum_{k,\mu,\nu} \frac{\mathcal{D}_{\mu\nu}(k)}{2} \delta\rho_{\mu}(k, \tau) \delta\rho_{\nu}(-k, \tau), \end{aligned} \quad (6.2)$$

where α runs over the inequivalent plaquette sublattices, $\mathcal{D}_{\mu\nu}(k)$ is the interaction matrix that follows from expanding the Hamiltonian terms $-2J\sqrt{\rho\rho\rho\rho\rho}$ and $V\rho\rho\rho$ to quadratic order, and ϕ is the lattice curl of Φ around each plaquette. In Fourier space, we have

$$\phi_{\alpha}(k) = 2i \sum_{\beta\gamma\delta} \varepsilon_{\alpha\beta\gamma\delta} \Phi_{\beta}(k) s_{\gamma} c_{\delta}, \quad (6.3)$$

where $\varepsilon_{\alpha\beta\gamma\delta}$ is the totally antisymmetric tensor, $c_{\mu} = \cos(ke_{\mu}/2)$, and $s_{\mu} = \sin(ke_{\mu}/2)$.

Since the two sublattices of the diamond lattice are inequivalent, there are two separate (large- S) constraints on ρ , one for each sublattice:

$$\sum_{l \in V_{r \in A}} b_l^{\dagger} b_l - S = 0, \quad \sum_{l \in V_{r \in B}} b_l^{\dagger} b_l - S = 0. \quad (6.4)$$

In Fourier space, these can be written as

$$\sum_{\mu} c_{\mu} \delta\rho_{\mu}(k) = \sum_{\mu} s_{\mu} \delta\rho_{\mu}(k) = 0; \quad (6.5)$$

since we have two constraints for the four fields $\delta\rho_{\mu}$, there are two independent fields left. Resolving the constraints explicitly, however, leads to rather intractable algebra; therefore, we only present the implicit approach of Sec. IIC.

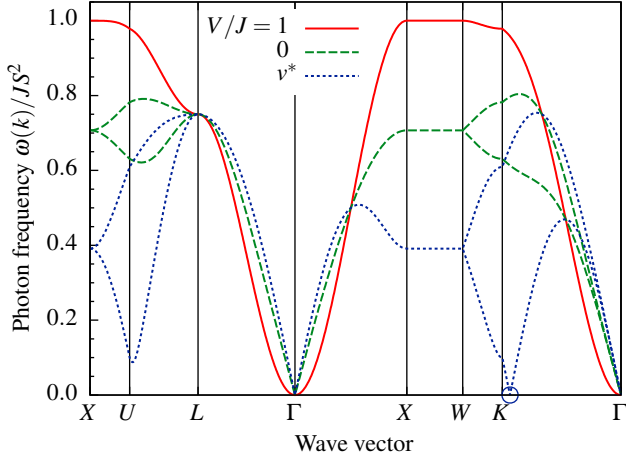


FIG. 11. Photon dispersion relation of the large- S QDM on the diamond lattice. The spectrum is gapless at the Γ point and has two non-degenerate branches away from the RK point. Another minimum develops for small V near the K points; however, a plaquette ordering transition occurs before this minimum would become unstable at $V/J = v^* \approx -0.694$.

Ignoring instantons (for the reasons discussed in Sec. III B), the middle term of Eq. (6.2) can be expanded about a given minimum of the cosine. After Fourier transforming and substituting (6.3), we obtain

$$\begin{aligned} \mathcal{S} = & \int d\tau \sum_{k,\mu} i\delta\rho_\mu(k, \tau) \partial_\tau \Phi_\mu(-k, \tau) \\ & + \int d\tau \sum_{k,\mu,\nu} \frac{M_{\mu\nu}}{2} \Phi_\mu(k, \tau) \Phi_\nu(-k, \tau) \\ & + \int d\tau \sum_{k,\mu,\nu} \frac{D_{\mu\nu}(k)}{2} \delta\rho_\mu(k, \tau) \delta\rho_\nu(-k, \tau); \end{aligned} \quad (6.6)$$

obtaining the matrices \mathcal{M} and \mathcal{D} from the QDM Hamiltonian is straightforward but algebraically tedious and is presented in App. C.

As in Sec. II C, the fields Φ_μ can now be integrated out to obtain the action

$$\begin{aligned} \mathcal{S} = & \frac{1}{2} \int d\tau \sum_{k,\mu,\nu} \left[(\mathcal{M}^{-1})_{\mu\nu} \partial_\tau \delta\rho_\mu(k, \tau) \partial_\tau \delta\rho_\nu(k, \tau) \right. \\ & \left. + \mathcal{D}_{\mu\nu}(k) \delta\rho_\mu(k, \tau) \delta\rho_\nu(-k, \tau) \right]. \end{aligned} \quad (6.7)$$

The dispersion $\omega^2(k)$ is given by the eigenvalues of the matrix $\mathcal{M}\mathcal{D}$. Two of these eigenvalues are identically zero: these correspond to the unphysical modes ruled out by the constraints (6.5). The remaining two eigenvalues can be worked out by straightforward but rather lengthy algebra; the resulting dispersion is plotted along high-symmetry directions for three values of V/J in Fig. 11.

Away from the RK point, the resulting two photon modes are normally non-degenerate; near $k = 0$, however, they agree

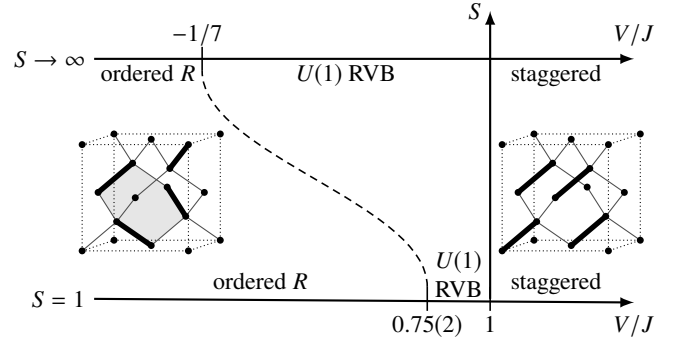


FIG. 12. Phase diagram of the diamond lattice quantum dimer model at $S = \infty$ (this work) and $S = 1$ [14].

to leading order:

$$\omega^2 \approx \frac{S^4}{6} J(J-V)k^2, \quad (6.8)$$

giving a speed of light

$$c = S^2 \sqrt{J(J-V)/6}. \quad (6.9)$$

This can be contrasted to the quantum Monte Carlo result for $S = 1$ in Refs. [13, 14], namely $c \approx \sqrt{0.8J(J-V)}$. We expect higher-order corrections in the $1/S$ expansion to substantially reduce this discrepancy [16].

The ground state of the $S \rightarrow \infty$ model was obtained as a function of V/J by comparing the large- S minimum energy of ordered and resonating phases suggested in the literature [13, 14, 33]. The resulting phase diagram is shown in Fig. 12, together with the $S = 1$ phase diagram obtained in Ref. [14]. Unlike the previous cases, no resonating solid phase is identified in either limit: both phase diagrams consist of staggered ordered, $U(1)$ liquid and ordered R [13] phases. The liquid phase is far larger for $S \rightarrow \infty$ than at $S = 1$: this is consistent with the intuition that soft dimers (and spins) favour fluctuating phases.

VII. RELATION TO OTHER FIELD THEORETIC APPROACHES

For quantum dimers models on bipartite lattices, field-theoretic approaches were already known in the literature. These include height mappings in two dimensions [8] and $U(1)$ gauge theory descriptions in three dimensions [9]. In this section, we briefly review them and discuss how they relate to our large- S representation. For simplicity, we focus on the square and cubic lattices.

A. Height mapping on the square lattice

In $S = 1$ dimer models, a height mapping can be constructed by assigning a height \tilde{h} to all plaquettes of the lattice, starting from a reference plaquette with $\tilde{h} = 0$. Going

clockwise around a vertex in the A sublattice (see Fig. 1), the height field changes by $-1/4$ on crossing a bond without a dimer and by $+3/4$ on crossing one with a dimer. Likewise, going clockwise around a vertex in the B sublattice, \tilde{h} changes by $-3/4$ and $+1/4$ on bonds with and without dimers, respectively. These numbers are the difference between the occupation of a given bond and the average occupation of all bonds, $1/4$. Therefore, this mapping can be generalised to the large- S case by requiring that

$$\Delta\tilde{h} = \pm\delta\rho, \quad (7.1)$$

where the sign depends on the direction in which the bond is traversed, as described above.

In order to coarse-grain this height description, it is useful to define the so-called magnetic field representation,

$$\vec{B}(r) = (B_x, B_y, 0), \quad B_\mu(r) = (-1)^{x+y} \delta\rho_\mu(r), \quad (7.2)$$

in which the height mapping (7.1) can be expressed as

$$B_\mu(e+r_\mu/2) = \tilde{h}[r+(e_\mu+\varepsilon_{\mu\nu}e_\nu)/2] - \tilde{h}[r+(e_\mu-\varepsilon_{\mu\nu}e_\nu)/2]. \quad (7.3)$$

In reciprocal space, the signs appearing in (7.2) have the effect of shifting the gapless point of the dispersion (2.20) from (π, π) to $(0, 0)$, that is, coarse-graining will capture the long-wavelength, low-frequency features of the gapless modes. In particular, (7.3) can be Fourier transformed to give

$$B_\mu(k) = 2i\varepsilon_{\mu\nu} \sin(k_\nu/2)\tilde{h}(k); \quad (7.4)$$

comparing with (2.22) immediately gives

$$\tilde{h}(k) = h[k + (\pi, \pi)] \implies \tilde{h}(r) = (-1)^{x+y}h(r), \quad (7.5)$$

where h is the single-component height field introduced in Sec. II D. This concludes the reconstruction of the height mapping for classical (nondynamical) dimer models.

To recover quantum dynamics, the conjugate variables Φ_μ and ϕ can be reexpressed as

$$\vec{\Phi}(r) = (\tilde{\Phi}_x, \tilde{\Phi}_y, 0), \quad \tilde{\Phi}_\mu(r) = (-1)^{x+y} \Phi_\mu(r) \quad (7.6)$$

$$\tilde{\phi}(r) = (-1)^{x+y} \phi(r), \quad (7.7)$$

which leads to Berry phase terms of the form

$$i \sum_{k,\mu} \delta\rho_\mu(k) \partial_\tau \Phi_\mu(-k) = i \sum_k \vec{B}(k) \cdot \partial_\tau \vec{\Phi}(-k) \quad (7.8)$$

$$i \sum_k h(k) \partial_\tau \phi(-k) = i \sum_k \tilde{h}(k) \partial_\tau \tilde{\phi}(-k). \quad (7.9)$$

Integrating $\tilde{\phi}$ out and coarse-graining (that is, focusing on small k) then yields the quadratic action (2.27).

B. Coulomb gauge theory on the cubic lattice

The key idea of the mapping discussed above is turning the lattice gauge field and its divergence-free condition (2.3) into

a coarse-grained, true vector field with $\nabla \cdot \vec{B} = 0$. Indeed, for small k , (7.4) reduces to

$$\vec{B}(k) = ik \times \vec{h}(k) \iff \vec{B} = \nabla \times \vec{h}, \quad (7.10)$$

where $\vec{h} = (0, 0, \tilde{h})$. Similarly, we now want to construct a divergence-free magnetic field \vec{B} on the cubic lattice by coarse-graining $\delta\rho_\mu$. To achieve this, we express our field in terms of a magnetic vector potential: $\vec{B} = \nabla \times \vec{A}$.

The construction again starts by defining

$$B_\mu(r) = (-1)^{x+y+z} \delta\rho_\mu(r); \quad (7.11)$$

similarly to the square lattice case, this amounts to shifting the gapless point of the photon dispersion from (π, π, π) to the origin. The reciprocal space constraint (3.3) now becomes

$$\sum_\mu 2i \sin(k_\mu/2) B_\mu(k) = 0. \quad (7.12)$$

This constraint can be resolved similarly to (7.4) by introducing another vector field \vec{A} :

$$B_\mu(k) = 2i\varepsilon_{\mu\nu\lambda} \sin(k_\nu/2) A_\lambda(k); \quad (7.13)$$

at small k , this reduces to $B = \nabla \times A$, as desired.

We now turn the conjugate variables Φ and ϕ into vector fields by writing

$$\vec{\Phi}_\mu(r) = (-1)^{x+y+z} \Phi_\mu(r) \quad (7.14)$$

$$\vec{\phi}_\mu(r) = (-1)^{x+y+z} \phi_\mu(r). \quad (7.15)$$

Eq. (3.7) can be written as

$$\vec{\phi}_\mu(k) = 2i\varepsilon_{\mu\nu\lambda} \sin(k_\nu/2) \vec{\Phi}_\lambda(k) \quad (7.16)$$

and the Berry phase can be integrated by parts to obtain

$$i \sum_{k,\mu} \delta\rho_\mu(k) \partial_\tau \Phi_\mu(-k) = i \sum_k \partial_\tau \vec{A}(k) \cdot \vec{\phi}(-k). \quad (7.17)$$

Expanding to quadratic order in ϕ around a given minimum of the cosine, we finally obtain the action

$$S = \int d\tau \sum_k \left[i \partial_\tau \vec{A}(k) \cdot \vec{\phi}(-k) + \frac{JS^2}{36} \vec{\phi}(k) \cdot \vec{\phi}(-k) + \frac{\tilde{\mathcal{D}}_{\mu\nu}}{2} A_\mu(k) A_\nu(-k) \right], \quad (7.18)$$

where $\tilde{\mathcal{D}}$ is given in terms of the matrix \mathcal{D} defined in (3.5) by

$$\tilde{\mathcal{D}}_{\mu\nu}(k) = 4\varepsilon_{\mu\rho\sigma} \varepsilon_{\nu\lambda\sigma} \sin(k_\rho/2) \sin(k_\lambda/2) \mathcal{D}_{\rho\sigma}[k + (\pi, \pi, \pi)]. \quad (7.19)$$

Finally, we integrate out ϕ and expand $\tilde{\mathcal{D}}$ around $q = 0$ to obtain a coarse-grained action in terms of A only. Away from the RK point, the leading order terms give

$$S \simeq \int d\tau \sum_k \left[\frac{9}{JS^2} \partial_\tau \vec{A}(k) \cdot \partial_\tau \vec{A}(-k) + 2(J - V) \vec{B}(k) \cdot \vec{B}(-k) \right]. \quad (7.20)$$

Similarly to ordinary quantum electrodynamics, we can identify $\partial_\tau \vec{A}$ as the electric field; that is, (7.20) is the action of a linearly dispersing $U(1)$ gauge theory. The speed of light is given by

$$c = \frac{S}{3} \sqrt{2(J - V)J}, \quad (7.21)$$

in agreement with (3.15). At the RK point, the B^2 term vanishes; to leading order, the action becomes

$$\mathcal{S} \simeq \int d\tau \sum_k \left\{ \frac{9}{JS^2} \partial_\tau \vec{A}(k) \cdot \partial_\tau \vec{A}(-k) - \frac{J}{2} [k \times \vec{B}(k)] \cdot [k \times \vec{B}(-k)] \right\}. \quad (7.22)$$

VIII. CONCLUSION

We proposed a general route to obtain the field-theoretic action for microscopic Hamiltonians with hard constraints, based on a slave boson representation of the relevant degrees of freedom and their constraints, combined with a large- S path integral formulation.

We used it to systematically derive Lagrangians for bipartite QDMs in 2D and 3D from the corresponding microscopic Hamiltonians. We find good agreement with known results in the literature; namely, calculations up to quadratic order yield a stiffness for the square lattice QDM at the RK point equal to 1/4 compared to the exact result $\pi/18$ [5, 12]; and they yield a speed of light in the gapless phase of the diamond lattice QDM $c = \sqrt{J(J - V)/6} S^2$ compared to the numerical result $c(S = 1) \simeq \sqrt{0.8J(J - V)}$ [13, 14].

Our approach applies straightforwardly to the nonbipartite case of the QDM on the triangular lattice, where we observe an intriguing analytical relation to the formalism of the cubic lattice, which will be interesting to explore in future work.

ACKNOWLEDGEMENTS

We thank Baptiste Bermond, John Chalker, and Roderich Moessner for useful discussions. A.M.T. is supported by the Condensed Matter Physics and Materials Science Division, in turn funded by the U.S. Department of Energy, Office of Basic Energy Sciences, under Contract No. DE-SC0012704. G.G. was supported by the U.S. Department of Energy, Office of Science, Basic Energy Sciences as a part of the Computational Materials Science Program. This work was supported, in part, by the Engineering and Physical Sciences Research Council (EPSRC) Grant No. EP/M007065/1 (C.C. and G.G.) and Grant No. EP/P034616/1 (C.C.). Statement of compliance with the EPSRC policy framework on research data: this publication reports theoretical work that does not require supporting research data.

Appendix A: Instanton measure on the square lattice

Instantons appear naturally in the compact gauge theory as stationary trajectories of the action with ϕ changing by 2π on a given site between $\tau = \pm\infty$. Unlike the point-like instantons described in Sec. IID 2, these objects are smooth as a function of time, and thus have a nontrivial instanton core. The action can then be expanded to quadratic order around such solutions, similarly to the case $h = \phi \equiv 0$ shown in Sec. IID 1. The resulting fluctuation determinant will appear in the probability of instantons as a preexponential factor.

We thus have to construct such a stationary instanton solution. Using (2.24, 2.29) with a single instanton event at $r = \tau = 0$, we get the following quadratic action in terms of Fourier components:

$$\mathcal{S} = \int (d\omega)(d^2k) \left\{ \omega h(k, \omega) \phi(-k, -\omega) + \frac{\mathcal{D}_0(k)}{2} h(k, \omega) h(-k, -\omega) + \frac{M}{2} \left[\phi(k, \omega) - \frac{2\pi i}{\omega} \right] \times \text{c.c.} \right\}, \quad (\text{A1})$$

where we introduce $M = JS^2/8$ for brevity and i/ω is the Fourier transform of the Heaviside function in τ . Since the different Fourier components are decoupled in this action, we can minimise with respect to them separately, resulting in the stationary action

$$h_0(k, \omega) = \frac{2\pi i q M}{\omega^2 + M \mathcal{D}_0(k)} \\ \phi_0(k, \omega) = \frac{2\pi i q}{\omega} \frac{M \mathcal{D}_0(k)}{\omega^2 + M \mathcal{D}_0(k)}. \quad (\text{A2})$$

In real space, this corresponds to a point-like instanton described in Sec. IID 2 together with a power-law decaying ‘‘instanton core.’’ We should also note that (A2) is not a stationary trajectory under the original action, but it becomes one if the $M(1 - \cos \phi)$ potential term is replaced with a continued parabolic potential, $V(\phi) = \frac{M}{2} \min_n (\phi - 2\pi n)^2$: Indeed, the only point where ϕ_0 reaches π is $r = \tau = 0$, where the cusp in the potential is recovered by the external instanton charge. In the following, we will thus use $V(\phi)$.

The action can now be expanded to quadratic order in δh and $\delta \phi$ around both the trivial trajectory $h = \phi \equiv 0$ and the instanton trajectory (A2). δh can easily be integrated out in both cases, giving the following actions in $\delta \phi$:

$$\delta \mathcal{S}_0 = \frac{1}{2} \int (d\omega)(d^2k) \left(\frac{\omega^2}{\mathcal{D}_0(k)} + M \right) \delta \phi(k, \omega) \delta \phi(-k, -\omega) \quad (\text{A3})$$

$$\delta \mathcal{S}_i = \delta \mathcal{S}_0 - \frac{\pi M}{\partial_\tau \phi_0(r = \tau = 0)} [\delta \phi(r = \tau = 0)]^2, \quad (\text{A4})$$

where the additional term in (A4) corresponds to the cusp of the continued parabolic potential at $\phi = \pi$, only reached at $r = \tau = 0$. The most important difference between the two actions is that $\delta \mathcal{S}_i$ has the zero mode $\psi = \partial_\tau \phi_0$, corresponding

to the continuous time-translation symmetry of the setup. For such modes, the usual contribution to the partition function, $e^{-\mathcal{S}_{\text{cl}}}(\det K)^{-1/2}$, is replaced by

$$d\tau \sqrt{\frac{\langle \psi | \psi \rangle}{2\pi}} e^{-\mathcal{S}_{\text{cl}}}(\det \tilde{K})^{-1/2}, \quad (\text{A5})$$

where \mathcal{S}_{cl} is the action due to the stationary instanton, given by (2.31), and \tilde{K} is the fluctuation kernel of (A4) restricted to the non-zero modes. Suppose $|\psi\rangle$ is proportional to a basis vector (this can always be achieved using a unitary transformation on the kernel K). Then, \tilde{K} is the principal minor of K that excludes the row and column of ψ . $\det \tilde{K}$ is thus a cofactor of the full kernel, and we have

$$\det \tilde{K} = \langle \tilde{\psi} | K^{-1} | \tilde{\psi} \rangle \det K \quad (\text{A6})$$

by the cofactor formula for matrix inversion, where $|\tilde{\psi}\rangle$ is the normalised zero mode $|\psi\rangle / \sqrt{\langle \psi | \psi \rangle}$.

In a matrix language, K is the sum of the kernel K_0 appearing in (A3) and a dyad $-\lambda|\nu\rangle\langle\nu|$, where $|\nu\rangle$ corresponds to the δ -function at $r = \tau = 0$ implied in (A4) in an arbitrary basis. For such a matrix, we have the following:

(i) $\det K = \det K_0(1 - \lambda\langle\nu|K_0^{-1}|\nu\rangle)$.

(ii) If $1 - \lambda\langle\nu|K_0^{-1}|\nu\rangle = 0$, $K_0^{-1}|\nu\rangle$ is an eigenvector of K with eigenvalue 0.

(iii) $K^{-1} = K_0^{-1} + \frac{\lambda K_0^{-1}|\nu\rangle\langle\nu|K_0^{-1}}{1 - \lambda\langle\nu|K_0^{-1}|\nu\rangle}$.

The first statement can be shown by inserting factors of $K_0^{1/2}K_0^{-1/2}$ into the definition of K ; the other two are straightforward to verify. Now, $\det \tilde{K}$ follows as

$$\det \tilde{K} = \left\langle \tilde{\psi}_0 \left| \left(K_0^{-1} + \frac{\lambda K_0^{-1}|\nu\rangle\langle\nu|K_0^{-1}}{1 - \lambda\langle\nu|K_0^{-1}|\nu\rangle} \right) \tilde{\psi}_0 \right\rangle \times \right. \\ \left. (1 - \lambda\langle\nu|K_0^{-1}|\nu\rangle) \det K_0 \quad (\text{A7}) \right.$$

$$= \langle \tilde{\psi}_0 | \lambda K_0^{-1} |\nu\rangle \langle \nu | K_0^{-1} | \tilde{\psi}_0 \rangle \det K_0 \\ = \lambda \langle \nu | K_0^{-2} | \nu \rangle \det K_0. \quad (\text{A8})$$

In the first line, we substitute statements (i) and (iii) into (A6); in the second, we note that $1 - \lambda\langle\nu|K_0^{-1}|\nu\rangle = 0$ in our case, so only the second term of K^{-1} gives any contribution [34]. Finally, we use that $|\tilde{\psi}_0\rangle$ is the normalised zero mode, so by statement (ii), it must be $K_0^{-1}|\nu\rangle / \sqrt{\langle\nu|K_0^{-2}|\nu\rangle}$. Altogether, the measure of the instanton solutions relative to that of the instanton-free solution, $(\det K_0)^{-1/2}$, is

$$d\tau \sqrt{\frac{\langle \psi | \psi \rangle}{2\pi\lambda\langle\nu|K_0^{-2}|\nu\rangle}} e^{-\mathcal{S}_{\text{cl}}}. \quad (\text{A9})$$

In the (k, ω) basis, K_0 is positive definite and diagonal, $K_0(k, \omega) = \omega^2/\mathcal{D}_0(k) + M$, $\lambda = 2\pi M/[\partial_\tau\phi_0(0, 0)]$, and

$\nu(k, \omega) = 1$ (the Fourier transform of a δ -function at the origin). It is easy to verify that $1 - \lambda\langle\nu|K_0^{-1}|\nu\rangle = 0$, that is, K indeed has a zero mode; furthermore, $K_0^{-1}|\nu\rangle \propto \partial_\tau\phi_0$, as expected. Substituting into (A9) then gives that the measure of instanton solutions of a given sign is μI , where $I = e^{-\mathcal{S}_0}$ and

$$\mu = \sqrt{M\pi} \int (d^2k) \omega(k); \quad (\text{A10})$$

at the RK point on the square lattice, $\mu = JS^{3/2} \sqrt{\pi/8}$.

Appendix B: Details of the calculation for the honeycomb lattice

Following from Sec. V, we express the bosonic operators in the radial gauge in the path integral formulation of the model. For $r \in A$:

$$b_{r,\eta} = \sqrt{\rho_\eta(r + e_\eta/2)} \exp[i\Phi_\eta(r + e_\eta/2)] \\ \equiv \sqrt{\frac{S}{3} + \delta\rho_\eta(r + e_\eta/2)} \exp[i\Phi_\eta(r + e_\eta/2)]. \quad (\text{B1})$$

For $r \in B$, the expressions are equivalent except for a change in sign, $+e_\eta/2 \rightarrow -e_\eta/2$. Notice that, by thinking of $\rho_\eta(r + e_\eta/2)$ and $\Phi_\eta(r + e_\eta/2)$ as functions defined on the midpoints of the bonds, there is no ambiguity nor redundancy in the notation.

The constraints in Eq. (5.2) can then be written (choosing for concreteness $r \in A$) as

$$\sum_\eta \delta\rho_\eta(r + e_\eta/2) = 0 \\ \delta\rho_1(r + e_1/2) + \delta\rho_2(r + e_1 - e_2/2) \\ + \delta\rho_3(r + e_1 - e_3/2) = 0. \quad (\text{B2})$$

Taking the Fourier transform with respect to sublattice A , the constraints take on a more symmetric form:

$$\sum_\eta e^{-ike_\eta/2} \delta\rho_\eta(k) = 0, \quad \sum_\eta e^{ike_\eta/2} \delta\rho_\eta(k) = 0, \quad (\text{B4})$$

where in the second line we divided out an overall factor e^{-ike_1} . More conveniently, we can add and subtract them to obtain

$$\sum_\eta c_\eta \delta\rho_\eta(k) = 0, \quad \sum_\eta s_\eta \delta\rho_\eta(k) = 0, \quad (\text{B5})$$

where again we used the shorthand notation $c_\eta = \cos(ke_\eta/2)$ and $s_\eta = \sin(ke_\eta/2)$. With three field variables $\delta\rho_\eta(k)$ and two constraints, we expect only one degree of freedom.

As we did for the square lattice, it is convenient not to attempt to resolve the constraint directly but rather consider first the argument of the cosine term in the Hamiltonian,

$$\tilde{\phi}(r) = \Phi_1(r + e_1/2) - \Phi_3(r + e_1 - e_3/2) + \Phi_2(r + e_1 - e_3 + e_2/2) \\ - \Phi_1(r + e_2 - e_3 + e_1/2) + \Phi_3(r + e_2 - e_3/2) - \Phi_2(r + e_2/2), \quad (\text{B6})$$

and its Fourier transform

$$\begin{aligned}\tilde{\phi}(k) &= \Phi_1(k)e^{-ike_1/2} - \Phi_3(k)e^{-ik(e_1-e_3)/2} + \Phi_2(k)e^{-ik(e_1-e_3+e_2)/2} \\ &\quad - \Phi_1(k)e^{-ik(e_2-e_3+e_1)/2} + \Phi_3(k)e^{-ik(e_2-e_3)/2} - \Phi_2(k)e^{-ike_2/2} \\ &= e^{ike_3} 2i [\Phi_1(k)(s_2c_3 - s_3c_2) + \Phi_2(k)(s_3c_1 - s_1c_3) + \Phi_3(k)(s_1c_2 - s_2c_1)].\end{aligned}\quad (\text{B7})$$

The nicely symmetric expression in Eq. (B7) required a few lines of algebra and the property of the lattice vectors $e_1 + e_2 + e_3 = 0$. As we inferred above from the constraints on the $\delta\rho_\eta$ fields, there is only one real scalar degree of freedom, and as before it is convenient to do away with the phase factor [effectively, use plaquette centres as reference points for $\phi(r)$] and define

$$\begin{aligned}\phi(k) &= e^{-ike_3} \tilde{\phi}(k) \\ &= 2i [\Phi_1(k)(s_2c_3 - s_3c_2) + \Phi_2(k)(s_3c_1 - s_1c_3) \\ &\quad + \Phi_3(k)(s_1c_2 - s_2c_1)].\end{aligned}\quad (\text{B8})$$

[Notice the importance of the factor of i in preserving the condition of Fourier transform of a real field, $\phi^*(k) = \phi(-k)$ due to the antisymmetric behaviour of the sine function.]

Finally, we look for a conjugate field $h(k)$ such that the Berry phase in the path integral can be written as $ih(k)\partial_\tau\phi(-k)$. Namely, we look for $h(k)$ that satisfies

$$h(k)\partial_\tau\phi(-k) = \sum_\eta \delta\rho_\eta(k)\partial_\tau\Phi_\eta(-k). \quad (\text{B9})$$

Substituting the expression for $\phi(k)$, Eq. (B8), into the equation above, we obtain

$$\begin{aligned}\delta\rho_1(k) &= -2i(s_2c_3 - s_3c_2)h(k) \\ \delta\rho_2(k) &= -2i(s_3c_1 - s_1c_3)h(k) \\ \delta\rho_3(k) &= -2i(s_1c_2 - s_2c_1)h(k).\end{aligned}\quad (\text{B10})$$

One can then straightforwardly verify that the introduction of the field $h(k)$ automatically resolves the constraints,

$$\sum_\eta c_\eta \delta\rho_\eta \propto [c_1(s_2c_3 - s_3c_2) + c_2(s_3c_1 - s_1c_3) + c_3(s_1c_2 - s_2c_1)]h(k) = 0 \quad (\text{B11})$$

$$\sum_\eta s_\eta \delta\rho_\eta \propto [s_1(s_2c_3 - s_3c_2) + s_2(s_3c_1 - s_1c_3) + s_3(s_1c_2 - s_2c_1)]h(k) = 0. \quad (\text{B12})$$

We are thus in the position to write the full large- S action of the system, including both the Berry phase and Hamiltonian contributions, in terms of the fields $h(k)$ and $\phi(k)$ only.

To obtain the Gaussian field theory for the honeycomb lattice QDM, it is convenient to rewrite $\cos(\phi) = 1 - [1 - \cos(\phi)]$

and notice that the term in square brackets contains only quadratic and higher-order contributions. Correspondingly, we can write

$$\sqrt{\rho\rho\rho\rho\rho\rho} \cos(\phi) \simeq \sqrt{\rho\rho\rho\rho\rho\rho} - \frac{S^3}{27} [1 - \cos(\phi)], \quad (\text{B13})$$

and focus on expanding to second order the first term on the right hand side, as well as the $V\rho\rho\rho$ terms in the Hamiltonian in Eq. (5.1). Linear terms in $\delta\rho_\eta(r + e_\eta/2)$ vanish upon summing over r because of the dimer constraint. After quite some algebra, one arrives at the following contributions to quadratic order:

$$\begin{aligned}&\frac{JS}{3} \left\{ \delta\rho_1(k)\delta\rho_1(-k)s_{23}^2 + \delta\rho_2(k)\delta\rho_2(-k)s_{31}^2 \right. \\ &\quad \left. + \delta\rho_3(k)\delta\rho_3(-k)s_{12}^2 \right\} \\ &- \frac{JS}{3} \left\{ [\delta\rho_1(k)\delta\rho_2(-k) + \text{c.c.}]c_{23}c_{31} \right. \\ &\quad + [\delta\rho_2(k)\delta\rho_3(-k) + \text{c.c.}]c_{31}c_{12} \\ &\quad \left. + [\delta\rho_3(k)\delta\rho_1(-k) + \text{c.c.}]c_{12}c_{23} \right\} \\ &+ \frac{VS}{3} \left\{ [\delta\rho_1(k)\delta\rho_2(-k) + \text{c.c.}](c_{23}c_{31} + s_{23}s_{31}) \right. \\ &\quad + [\delta\rho_2(k)\delta\rho_3(-k) + \text{c.c.}](c_{31}c_{12} + s_{31}s_{12}) \\ &\quad \left. + [\delta\rho_3(k)\delta\rho_1(-k) + \text{c.c.}](c_{12}c_{23} + s_{12}s_{23}) \right\},\end{aligned}\quad (\text{B14})$$

where we introduced

$$\begin{aligned}s_{\mu\nu} &= \sin[k(e_\mu - e_\nu)/2] = s_\mu c_\nu - s_\nu c_\mu \\ c_{\mu\nu} &= \cos[k(e_\mu - e_\nu)/2] = c_\mu c_\nu + s_\mu s_\nu\end{aligned}\quad (\text{B15})$$

for convenience. Substituting the expressions (B10) of $\delta\rho_\eta(k)$ in terms of $h(k)$, and ignoring trivial constants, we obtain the action given in Eq. (5.4) in Sec. V.

Appendix C: Details of the calculation for the diamond lattice

The interaction matrix $\mathcal{D}_{\mu\nu}$ can be obtained in much the same way as for the honeycomb lattice, see Appendix. B. For plaquettes in the $\mu = 1, 2, 3$ sublattice, we obtain the contribu-

$$\begin{aligned}&\frac{JS}{4} \left\{ \delta\rho_1(k)\delta\rho_1(-k)s_{23}^2 + \delta\rho_2(k)\delta\rho_2(-k)s_{31}^2 + \delta\rho_3(k)\delta\rho_3(-k)s_{12}^2 \right. \\ &\quad - [\delta\rho_1(k)\delta\rho_2(-k) + \delta\rho_2(k)\delta\rho_1(-k)]c_{23}c_{31} - [\delta\rho_2(k)\delta\rho_3(-k) + \delta\rho_3(k)\delta\rho_2(-k)]c_{31}c_{12} \\ &\quad \left. - [\delta\rho_3(k)\delta\rho_1(-k) + \delta\rho_1(k)\delta\rho_3(-k)]c_{12}c_{23} \right\}\end{aligned}$$

$$\begin{aligned}
& + \frac{VS}{4} \left\{ [\delta\rho_1(k)\delta\rho_2(-k) + \delta\rho_2(k)\delta\rho_1(-k)](c_{23}c_{31} + s_{23}s_{31}) + [\delta\rho_2(k)\delta\rho_3(-k) + \delta\rho_3(k)\delta\rho_2(-k)](c_{31}c_{12} + s_{31}s_{12}) \right. \\
& \left. + [\delta\rho_3(k)\delta\rho_1(-k) + \delta\rho_1(k)\delta\rho_3(-k)](c_{12}c_{23} + s_{12}s_{23}) \right\}, \tag{C1}
\end{aligned}$$

where we again introduced $c_{\mu\nu} = \cos[k(e_\mu - e_\nu)/2] = c_\mu c_\nu + s_\mu s_\nu$ and $s_{\mu\nu} = \sin[k(e_\mu - e_\nu)/2] = s_\mu c_\nu - c_\mu s_\nu$. The other three sublattices of plaquettes give rise to equivalent contributions with $123 \leftrightarrow 234 \leftrightarrow 341 \leftrightarrow 412$. Now, the matrix \mathcal{D} can be written explicitly as

$$\mathcal{D} = \frac{JS}{2} \mathcal{J} + \frac{VS}{2} \mathcal{V} \tag{C2}$$

$$\mathcal{J} = \begin{pmatrix} s_{23}^2 + s_{34}^2 + s_{43}^2 & -(c_{13}c_{23} + c_{14}c_{24}) & -(c_{12}c_{32} + c_{14}c_{34}) & -(c_{12}c_{42} + c_{13}c_{43}) \\ -(c_{23}c_{13} + c_{24}c_{14}) & s_{34}^2 + s_{41}^2 + s_{13}^2 & -(c_{21}c_{31} + c_{24}c_{34}) & -(c_{21}c_{41} + c_{23}c_{43}) \\ -(c_{32}c_{12} + c_{34}c_{14}) & -(c_{31}c_{21} + c_{34}c_{24}) & s_{41}^2 + s_{12}^2 + s_{24}^2 & -(c_{31}c_{41} + c_{32}c_{42}) \\ -(c_{42}c_{12} + c_{43}c_{13}) & -(c_{41}c_{21} + c_{43}c_{23}) & -(c_{41}c_{31} + c_{42}c_{32}) & s_{12}^2 + s_{23}^2 + s_{31}^2 \end{pmatrix} \tag{C3}$$

$$\mathcal{V} = \begin{pmatrix} 0 & c_{13}c_{23} - s_{13}s_{23} + c_{14}c_{24} - s_{14}s_{24} & c_{12}c_{32} - s_{12}s_{32} + c_{14}c_{34} - s_{14}s_{34} & c_{12}c_{42} - s_{12}s_{42} + c_{13}c_{43} - s_{13}s_{43} \\ c_{23}c_{13} - s_{23}s_{13} + c_{24}c_{14} - s_{24}s_{14} & 0 & c_{21}c_{31} - s_{21}s_{31} + c_{24}c_{34} - s_{24}s_{34} & c_{21}c_{41} - s_{21}s_{41} + c_{23}c_{43} - s_{23}s_{43} \\ c_{32}c_{12} - s_{32}s_{12} + c_{34}c_{14} - s_{34}s_{14} & c_{31}c_{21} - s_{31}s_{21} + c_{34}c_{24} - s_{34}s_{24} & 0 & c_{31}c_{41} - s_{31}s_{41} + c_{32}c_{42} - s_{32}s_{42} \\ c_{42}c_{12} - s_{42}s_{12} + c_{43}c_{13} - s_{43}s_{13} & c_{41}c_{21} - s_{41}s_{21} + c_{43}c_{23} - s_{43}s_{23} & c_{41}c_{31} - s_{41}s_{31} + c_{42}c_{32} - s_{42}s_{32} & 0 \end{pmatrix}. \tag{C4}$$

We can express the matrices \mathcal{J} and \mathcal{V} more concisely by introducing the matrix C with entries $c_{\mu\nu}$, the diagonal matrix \mathcal{R} with entries $\mathcal{R}_{\mu\mu} = \sum_\nu \cos[k(e_\mu - e_\nu)] - 2$, and defining $\Omega = \sum_{\mu < \nu} s_{\mu\nu}^2$:

$$\mathcal{J} = \Omega \mathbb{I} + \mathcal{R} - C^2 + 2C \tag{C5}$$

$$\mathcal{V} = 2C^2 - 6C - \mathcal{R}, \tag{C6}$$

where \mathbb{I} is the identity matrix.

Ignoring instantons, the middle term of Eq. (6.2) can be expanded about a given minimum of the cosine, giving

$$\frac{JS^3}{64} \sum_{\alpha,r} \phi_\alpha^2(r, \tau) = \frac{JS^3}{64} \sum_{\alpha,k} |\phi_\alpha(k, \tau)|^2 = \tag{C7}$$

$$\frac{JS^3}{64} \sum_{k,\mu\nu\alpha} \mathcal{Z}_{\alpha\mu}(k) \mathcal{Z}_{\alpha\nu}(-k) \Phi_\mu(k, \tau) \Phi_\nu(-k, \tau),$$

where $\mathcal{Z}_{\mu\nu} = 2i\varepsilon_{\mu\nu\lambda k} s_\lambda c_k$, see Eq. (6.3). Defining the matrix

$$\mathcal{M} = \frac{JS^3}{32} \mathcal{Z}^T(-k) \mathcal{Z}(k) = \frac{JS^3}{32} \mathcal{Z}^2, \tag{C8}$$

the quadratic action can now be written in the form (6.6).

The dispersion $\omega^2(k)$ is given by the eigenvalues of the matrix $\mathcal{M}\mathcal{D}$. It is important to note that $\mathcal{Z}_{\mu\nu}c_\nu = \mathcal{Z}_{\mu\nu}s_\nu = 0$ by the definition of \mathcal{Z} . Consequently, $\mathcal{M}\mathcal{C} = 0$, which greatly simplifies the form of $\mathcal{M}\mathcal{D}$. All in all, one has to diagonalise the matrix

$$\frac{JS^4}{64} [\Omega \mathcal{J} \mathcal{Z}^2 + (J - V) \mathcal{Z} \mathcal{R} \mathcal{Z}]. \tag{C9}$$

It follows from the definition of \mathcal{Z} that c_μ and s_μ (understood as 4-dimensional vectors) are eigenvectors of this matrix with zero eigenvalue. These correspond to the unphysical modes ruled out by the constraint (6.5).

- [1] A. Szabó and C. Castelnovo, Phys. Rev. B **100**, 014417 (2019).
- [2] D. S. Rokhsar and S. A. Kivelson, Phys. Rev. Lett. **61**, 2376 (1988).
- [3] D. H. Lee and S. A. Kivelson, Phys. Rev. B **67**, 024506 (2003).
- [4] P. Fulde, K. Penc, and N. Shannon, Ann. Phys. **11**, 892 (2002).
- [5] R. Moessner and K. S. Raman, *Quantum Dimer Models*, in *Introduction to Frustrated Magnetism*, edited by C. Lacroix, P.

- Mendels, and F. Mila, Springer Series in Solid-State Sciences Vol. 164 (Springer, Berlin, 2011).
- [6] D. A. Huse, W. Krauth, R. Moessner, and S. L. Sondhi, Phys. Rev. Lett. **91**, 167004 (2003).
- [7] R. Moessner and S. L. Sondhi, Phys. Rev. B **68**, 184512 (2003).
- [8] E. Fradkin, *Field Theories of Condensed Matter Physics* (Cambridge University Press, Cambridge, 2013).

- [9] C. L. Henley, *Annu. Rev. Cond. Matt. Phys.* **1**, 179 (2010).
- [10] C. L. Henley, *J. Stat. Phys.* **89**, 483 (1997).
- [11] E. Fradkin, D. A. Huse, R. Moessner, V. Oganesyan, and S. L. Sondhi, *Phys. Rev. B* **69**, 224415 (2004).
- [12] Y. Tang, A. W. Sandvik, and C. L. Henley, *Phys. Rev. B* **84**, 174427 (2011).
- [13] O. Sikora, F. Pollmann, N. Shannon, K. Penc, and P. Fulde, *Phys. Rev. Lett.* **103**, 247001 (2009).
- [14] O. Sikora, N. Shannon, F. Pollmann, K. Penc, and P. Fulde, *Phys. Rev. B* **84**, 115129 (2011). Note that the speed of light given in Eq. (26) in this reference was rescaled to match the different unit of length used in our work (nearest neighbour distance instead of half the cubic lattice constant).
- [15] G. Goldstein, C. Chamon and C. Castelnovo, *Phys. Rev. B* **95**, 174511 (2017).
- [16] M. P. Kwasigroch, B. Douçot, and C. Castelnovo, *Phys. Rev. B* **95**, 134439 (2017).
- [17] A. M. Polyakov, *Phys. Lett. B* **59**, 82 (1975).
- [18] S. Papanikolaou, E. Luijten, and E. Fradkin, *Phys. Rev. B* **76**, 134514 (2007).
- [19] S. Sachdev, *Phys. Rev. B* **40**, 5204 (1989).
- [20] P. W. Leung, K. C. Chiu, and K. J. Runge, *Phys. Rev. B* **54**, 12938 (1996).
- [21] C. Zeng and C. L. Henley, *Phys. Rev. B* **55**, 14935 (1997).
- [22] O. F. Syljuåsen, *Phys. Rev. B* **73**, 245105 (2006).
- [23] A. Ralko, D. Poilblanc, and R. Moessner, *Phys. Rev. Lett.* **100**, 037201 (2008).
- [24] D. Banerjee, M. Bögli, C. P. Hofmann, F.-J. Jiang, P. Widmer, and U.-J. Wiese, *Phys. Rev. B* **90**, 245143 (2014); *Phys. Rev. B* **94**, 115120 (2016).
- [25] T. Oakes, S. Powell, C. Castelnovo, A. Lamacraft, and J. P. Garrahan, *Phys. Rev. B* **98**, 064302 (2018).
- [26] J. Herzog-Arbeitman, S. Mantilla, and I. Sodemann, *Phys. Rev. B* **99**, 245108, (2019).
- [27] Instantons that do not obey this constraint also exist and give rise to pairs of Dirac quantised magnetic monopoles [28]. These monopoles are gapped quasiparticles and they only renormalise the low-energy theory through ring-exchange processes that obey the constraint (3.20).
- [28] M. Hermele, M. P. A. Fisher, and L. Balents, *Phys. Rev. B* **69**, 064404 (2004).
- [29] Curiously, in this case the condition that reduces the three cosine terms to two is the fact that one can decompose a hexagonal cell on the triangular lattice into 6 overlapping plaquettes; the product of the resulting 6 plaquette-flipping operators amounts to the identity. Indeed, these 6 plaquettes can be viewed as the 6 faces of a cube projected onto a plane down one of its body diagonals.
- [30] R. Moessner and S. L. Sondhi, *Phys. Rev. Lett.* **86**, 1881 (2001).
- [31] R. Moessner, S. L. Sondhi, and P. Chandra, *Phys. Rev. B* **64**, 144416 (2001).
- [32] T. M. Schlittler, R. Mosseri, and T. Barthel, *Phys. Rev. B* **96**, 195142 (2017).
- [33] N. Shannon, O. Sikora, F. Pollmann, K. Penc, and P. Fulde, *Phys. Rev. Lett.* **108**, 067204 (2012).
- [34] Note that, since $1 - \lambda \langle \nu | K_0^{-1} | \nu \rangle = 0$ due to the presence of the zero mode, both terms in (A7) are ill-defined. However, both are finite for any other λ , so we can formally evaluate it elsewhere and take the limit of λ going to its physical value. The divergence due to $1 - \lambda \langle \nu | K_0^{-1} | \nu \rangle = 0$ cancels, so the correct limit is indeed given by (A8).